STRUCTURAL ANALYSIS OF REINFORCED CONCRETE COLUMNS SUBJECTED TO UNDERWATER EXPLOSIONS

by

Jacob Sanders
A Thesis
Submitted to the
Graduate Faculty
of
George Mason University
in Partial Fulfillment of
The Requirements for the Degree
of
Master of Science
Civil and Infrastructure Engineering

Committee:

___________________________________ Dr. Girum Urgessa, Thesis Director

___________________________________ Dr. Doaa Bondok, Committee Member

___________________________________ Dr. David Lattanzi, Committee Member

___________________________________ Dr. Sam Salem, Department Chair

Date:______________________________ Summer Semester 2022
George Mason University
Fairfax, VA

Structural Analysis of Reinforced Concrete Columns Subjected to Underwater Explosions

A Thesis submitted in partial fulfillment of the requirements for the degree of Master of Science of Civil and Infrastructure Engineering at George Mason University

by

Jacob Sanders
Bachelor of Science
George Mason University, 2020

Director: Girum Urgessa, Associate Professor
Sid and Reva Dewberry Department of Civil and Infrastructure Engineering

Summer Semester 2022
George Mason University
Fairfax, VA

DEDICATION

This is dedicated to my family and friends who have helped and supported me every step of the way during the manifestation of this thesis.

ACKNOWLEDGEMENTS

I would like to thank the many friends, relatives, and supporters who have made this happen. My mother and father helped me with choosing a path. My academic advisor, Dr. Girum Urgessa, supported me throughout the process and guided me through the writing. My friends kept me sane throughout writing and writer's block. I would also like to thank the academic committee for their advice and review of my work.

TABLE OF CONTENTS

Page

LIST OF TABLES

LIST OF FIGURES

LIST OF EQUATIONS

ABSTRACT

STRUCTURAL ANALYSIS OF REINFORCED CONCRETE COLUMNS SUBJECTED TO UNDERWATER EXPLOSIONS

Jacob Sanders, M.S.

George Mason University, 2022

Thesis Director: Dr. Girum Urgessa

This thesis presents a study on structural modeling of reinforced concrete (RC) columns subjected to underwater explosions (UNDEX). With the heightened tensions stemming from warfare as well as accidents such as gas explosions or construction overblasting, understanding of UNDEX is critical to minimizing damage to infrastructure and human lives. Previous research was motivated by defense and is still a driving factor for blast research in the current day. Physical experimentation of UNDEX is expensive and computational analysis plays an important role in analyzing structures subjected to UNDEX.

Published research on the effect of UNDEX in civil engineering structures is relatively scant. This thesis provides a review of current literature concerning UNDEX effects, a proposed computational framework for assisting simulation of UNDEX effects, and a series of validation and sensitivity studies to examine a concrete material model in

a finite element analysis focused on reinforced columns. First, a literature review discussing the current understanding of UNDEX phenomena and effects on concrete structures is explored with considerations towards computational methods. Then a computational framework used to analyze complex loadings in ABAQUS is discussed. Additionally, an examination of empirical pressure equations used for dynamic analysis is presented and compared with existing experimental data. Lastly, the concrete damage plasticity (CDP) model is examined with sensitivity studies conducted on its input parameters. The effect of varying CDP input parameters on maximum displacement response is outlined.

CHAPTER ONE

1.1 - Motivation

The threat of terrorism attacks and accidents, such as gas explosions or construction overblasting on civil infrastructure, have increased in recent years. Research into the effects of underwater explosions (UNDEX) largely began in World War II due to the war effort. Much of this research, including fundamental equations and observations, was compiled into widely accessible work by the efforts of Cole and Weller [1]. The need for understanding UNDEX has remained critical due to its effects on infrastructure and human lives.

While the effect of air blast on civil infrastructure is studied to a greater length, published research on the effect of UNDEX in civil engineering structures is relatively scant. The widely available studies are mainly focused on UNDEX effects on ships. While these studies have clear applications in development of anti-blast properties for ship design and effective blast instruments, they remain largely irrelevant to civil engineering structures beyond the analysis of the generic UNDEX event and the pressure profiles it generates.

Additionally, most published work detailing effects of blast on civil engineering structures revolves mainly around air blast effects. This highlights a gap in present literature where there is a distinct lack of UNDEX research on the effects of structures in open literature. This thesis provides a comprehensive collection of current UNDEX research on structures and seeks to augment the current knowledge present in UNDEX literature through the exploration of its structural effects on structures, more specifically reinforced concrete (RC) structures due to its ubiquity in maritime or submerged structures.

One potential form of analysis for UNDEX is uncoupled analysis. This involves a decoupling of each step of the process between acquisition of raw data to finishing with a full response profile. In analytical scenarios for emergency situations, data can be fragmented or otherwise missing, creating a need for an analytical process that spans from processing full scenario data to working with original data. This analytical form is possible to create through usage of scripting and integration of an FEA program with a computational fluid dynamics (CFD) program in the case of UNDEX analysis. Potential challenges with developing this analytical form involve integrating the steps of this process so that the workflow is seamless and able to start at any point inside the process.

With the creation of an uncoupled analysis workflow, development on a fast-running model is also possible. While ideally full analysis would be done in a given scenario, emergencies and time-constrained situations create a need for a fast-running analytical model. Through the creation of data approximated from experimental results, the uncoupled analysis process can start from nearly the end with the input of data into the FEA program.

1.2 - Significance/Contribution

The contribution of this thesis is the development of an UNDEX loading scheme using MATLAB scripts to facilitate 3-D modeling of RC columns in ABAQUS and the subsequent investigation of the response of several RC columns subjected to UNDEX. There is a need to facilitate an uncoupled or partitioned structural analysis by importing pressure profile data from a computational fluid dynamics (CFD) code and applying it to models developed in FEA programs such as ABAQUS or ANSYS. One approach is through the use of scripts that automatically format retrieved data such that it can be easily uploaded by a user with relative ease. This thesis provides the development of MATLAB scripts connecting data received through CFD into a file readable by ABAQUS through MATLAB scripting.

The scripts are a key component to automating the process of creating complex loading scenarios on structures where each individual element in the structure is under a different loading amplitude. The scripts are able to aggregate every loading definition for each element and combine it into a single file that can be uploaded into ABAQUS as a full loading definition for a model. The framework developed in this thesis can be extended further by a process in which MATLAB can create full models along with the element definitions. The developed framework in this thesis compliments other efforts that are aimed at incorporation of CFD outputs in ABAQUS directly.

This thesis also investigated empirical pressure equations used for dynamic analysis and provided comparison with existing experimental data. The purpose of this analysis is to increase confidence in usage of empirical equations for examining dynamic loading scenarios. Furthermore, the concrete damage plasticity (CDP) model is examined and the effect of varying its input parameters on maximum displacement response is outlined. Understanding the effects of the CDP parameters will allow for more accurate and variable representations of concrete to be used for computational simulations.

1.3 - Thesis Organization

This thesis is divided into 5 separate chapters. Chapter 1 describes the motivation and overarching contribution of the research. The chapter also describes the structure of the thesis.

Chapter 2 presents a literature review. While the review focuses on the structural effects of UNDEX events on RC columns, it provides a broad overview of the research of UNDEX on various structures such as ships and dams. Additionally, the processes used to analyze UNDEX, such as the mechanics of UNDEX and computational methods, are covered.

Chapter 3 documents the initial research conducted beyond literature review. This involves basic modeling in ABAQUS, a 3-D modeling program with a focus on FEA, and earlier validations. Two documents from the literature review align closely with this thesis and thus are used as guidelines for modeling RC columns. While these models are not the main focus of the thesis, they were used to reinforce confidence in using ABAQUS.

Chapter 4 describes the computational methods used to analyze structures in ABAQUS. Due to the way that the models are constructed, each element in the structure can be assigned a separate loading from all the other elements. This allows for complex loading scenarios such as UNDEX to be explored in an efficient manner. This is accomplished through the development of MATLAB scripts that process loading definitions for each element and creates a singular file that can be uploaded into ABAQUS. The intricacies of this process are described in this chapter.

Chapter 5 details a dynamic validation study and a series of sensitivity studies on CDP parameters. Using empirical equations, displacement of the center node of the front face of an RC column model subjected to blast loading is compared to published experimental values. Additionally, sensitivity studies on variations of the concrete damage plasticity (CDP) parameters were conducted. These studies similarly examined the RC column model's front-facing center node and displacements of the node were compared during the studies.

Chapter 6 concludes the thesis. Discussion of the main findings of the contents of this thesis is conducted in this chapter. Additionally, limitations of the research conducted for this thesis and avenues for further research are also explored in this chapter.

CHAPTER TWO

2.1 - Introduction

This chapter presents the fundamentals of UNDEX, the physical and computational methods of analyzing its parameters, and the effects of UNDEX on select structures such as reinforced concrete dams and columns. First, the physical background and mechanics of UNDEX are discussed. Second, the methods of physical and computational modeling are covered. Third, a series of experiments based on various structures are discussed with a focus on concrete and RC-based structures. Lastly, concluding thoughts as well as potential direction for further research are covered.

2.2. Physical Background of UNDEX

At the beginning of every UNDEX event is the detonation of the explosive charge. After the initial detonation, the major event of an UNDEX event is the initial shock wave. When the explosive charge is detonated, a pressure wave is released from the charge location and expands outwards in a roughly spherical shape with the gas bubble following behind as shown in Figure 2.1 [2]. This pressure wave moves at such a speed that it is considered a shock wave and exerts a large amount of pressure on any point or surface it encounters. This shock wave travels at a highly nonlinear rate while still within 2–3 charge radii of the charge, and then moves linearly past that threshold [3].

Shock waves decay over time with their pressure values decreasing exponentially in the initial stages. Thus, the shock wave's loading effects decrease with increased distance between the point or surface of interest and the charge distance, otherwise known as the stand-off distance.

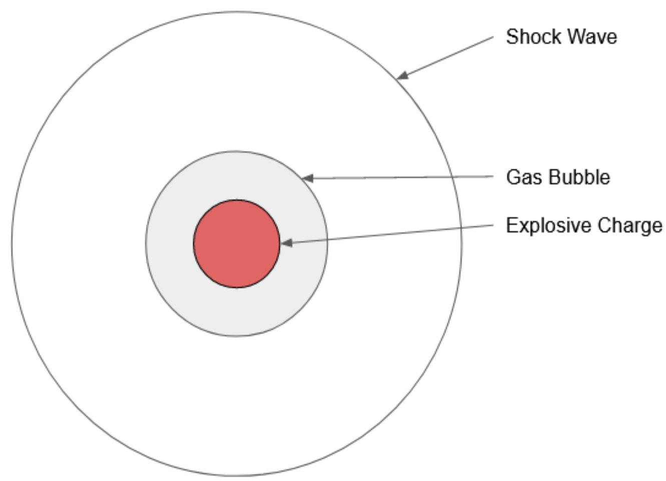

Figure 2.1. Diagram of shockwave and gas bubble propagation—reproduced from [2].

In the case of shock waves impacting on a surface or interface, such as a concrete slab or the boundary between air and water, a reflected wave is produced. This reflected wave will 'bounce' back away from the impacted surface and propagate outwards, similar to the original shock wave. The properties of this reflected wave vary on the impedance difference between the surface and the medium that the shockwave was traveling through. Figure 2.2 displays the typical pressure-time history of an UNDEX pressure wave, where the P_m term references the peak pressure, θ is the time constant, and $P_{m/e}$ references the pressure at which the time constant is reached [4]. As seen, the pressure decays exponentially until the time constant is reached, then decays at a slower rate until it completely dissipates. Costanzo [2], as shown in Figure 2.3, provided details of a reflected wave originating from an UNDEX event and reflecting off the air–water interface that has a tensile characteristic as opposed to the normal compressive characteristic. This is important because the reflected wave hits the analysis point of interest and lessens any compressive load placed on it from the original shock wave. This phenomenon is critical to the bulk cavitation effect discussed later.

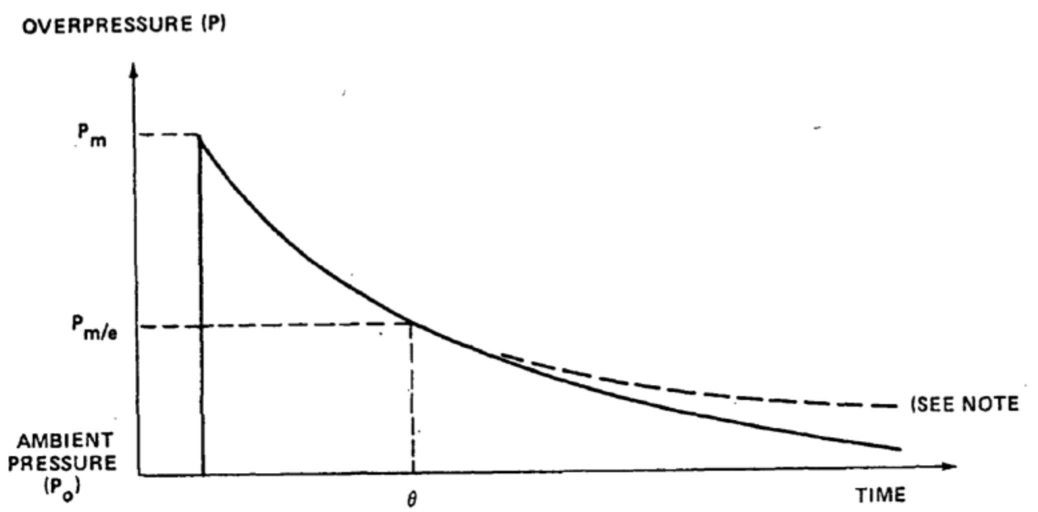

Figure 2.2: Diagram of Sample UNDEX Pressure-Time History

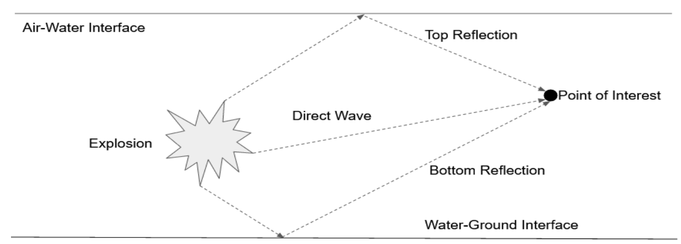

Figure 2.3. Diagram of a Reflected Shock wave bouncing off the Air-Water Interface—Reproduced from [2].

Once the initial shock wave has propagated away, the second part of the UNDEX event begins. As the gases left over from the explosion expand, the hydrostatic pressure of the water begins to bear down on the gases and shrink the gas bubble. When a threshold of shrinkage is reached, the gas bubble pushes back against the water and a shock wave is produced. This shock wave is called a bubble pulse. This cycle repeats itself and the gas bubble moves towards the air–water interface. This cycle continues with the gas bubble reaching a smaller peak radius value each time until either the gas bubble breaks or the gas vents towards the surface [4]. Figure 2.4 shows this cycle of expansion and compression of the gas bubble. Note that the effects of each subsequent pulse are lessened due to the dispersion of energy from the previous pulse.

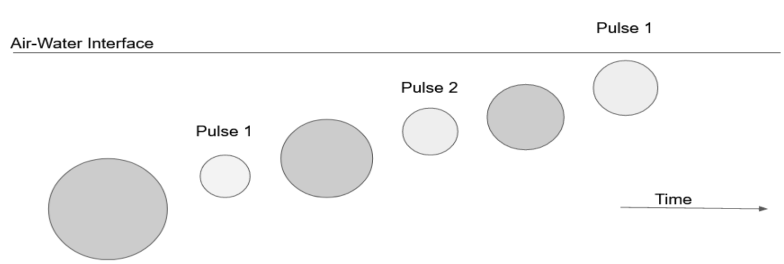

Figure 2.4. Multiple bubble pulses rising to the surface in succession—reproduced from [4].

While not considered in all UNDEX shock wave analyses, the impulse delivered from the repeated bubble pulses can be equal to or exceed that of the shock wave [5]. It is noteworthy that the presence of structures can exacerbate the effect of the bubble pulse due to the bubble developing a water jet, which increases its loading properties [5].

The last major phenomenon in UNDEX is cavitation. While the main focus of this chapter is on structural response, understanding the response of the surrounding water is also critical. If water is subjected to enough tensile energy originating from reflected shock waves off of the surface interface, the water cavitates and is unable to transmit any more shock. This cavitated region of water eventually collapses in a motion similar to that of a zipper, creating its own shockwave [2]. Like the bubble pulse, this phenomenon is not typically observed in simulations. However, unlike the bubble pulse, this may be due to the decreased prevalence of cavitation. Not every situation will involve explosives that output such energy that the reflected waves are enough to cavitate the water state. However, for larger structures in which a large quantity of explosive is certainly within the realm of study such as a ship, cavitation can be an important factor. For instance, the research of Ming et al. on ship structures examined the cavitation effects on the ship plating. It was found that the cavitation led to strain relaxation in the areas it affected [6]. Overall, the research on cavitation effects is less reported in literature than that of shock wave effects.

2.3 - Testing and Analysis

2.3.1 - Experimental Testing

The standard setup for testing UNDEX effects is having the tested material submerged in water with pressure gauges placed around it either attached to the surface of the tested material or a specified distance away from the material. The explosive is then placed depending on the circumstance either on the surface or at a certain stand-off distance away. Some experimental setups make use of high-speed cameras as another form of data gathering; however, they provide additional challenges such as water clarity, low light levels, and potential damage to the camera [7]. Once the experiment setup is verified, the experiment begins by detonating the explosive and measuring the quantities of the analyzed material through the sensors mounted. These setups then translate to data used either for analysis based on parameters, such as damage or displacement analyses, or used as validation for computational or numerical models [7]. In terms of the data gathered, pressure-time data, displacement-time data, and strain-time data are common for analyzing the effects of UNDEX.

Logistically, as useful as physical data would be from a full-scale experiment, it is unwieldy to physically test UNDEX effects on full-sized structures such as ships or dams. The financial costs, the difficulty of multiple trials, and potential unforeseen damages create an environment where that sort of experimentation is too unwieldy. Through the testing of physical models, research can be done on smaller scales. However, other issues can arise from effectively shrinking the experimental bounds, specifically scaling for testing involving concrete structures. Due to the nonlinear nature of concrete [8], a certain amount of scaling is required between the concrete and the explosive charge used [9].

Centrifuge testing can also be used in conjunction with the tested model and charge to create behavior similar to a larger, more realistic model [9]. This is done through a series of scaling laws that relate the physical model to the real-life equivalent [10]. Typically, this is done with dam models as it is suitable for scaled-down experiments.

When gathering physical data from physical experiments, some form of data-gathering equipment or measurement is imperative. In the case of UNDEX effects, sensors are typically used for measurement [8]. The types of sensors used vary based on the application; however, the usual sensors include pressure sensors and some combination of displacement, stress, and strain sensors. This is the standard suite of data points that are gathered for an analysis of UNDEX on a structure. Most reviewed papers do not mention the specific sensor brands; however, the configuration of these sensors is critical as knowing the relative positions of the charge, structure, and sensor creates a better picture of the scenario. Thus, the sensor configuration is typically included.

The beginning stage of the UNDEX experimental testing starts with the explosive charge. The detonation of the charge is an exothermic chemical reaction that propagates once it has started [2]. This chemical reaction creates extreme heat and pressure that move outwards in a wave originating from the charge location [2]. The intensity of these effects depends on the charge itself, specifically the type, mass, and shape. Table 2.1 shows a series of explosive types with their chemical formulas, density, and detonation velocity. TNT is mainly employed for experimentation, noted for its use for 'comparing energy and impulse yields of the other types of explosives' [2]. RDX is another explosive used for experimentation. Many of the other explosives are varying forms of TNT or RDX with additives added for performance, such as aluminum for longer burn times. The effect of mass is simple for explosive energy; the more mass present at detonation, the more explosive energy is released and, thus, higher levels of pressure and heat are achieved.

Table 2.1. Standard explosives with chemical composition, density, and detonation velocity [2].

Explosive	Formula	Density (g/cc)	Detonation Velocity (m/s)
TNT	$C_7H_5N_3O_6$	1.60	6940
RDX	$C_3H_6N_6O_6$	1.57	8940
Comp B	RDX/TNT/WAX 59.4/39.6/1.0	1.68	7900
H-6	RDX/TNT/AL/WAX 45.1/29.2/21.0/4.7	1.74	7440
PBXN-103	AP/AL/PNC/MTN/ RESOURCINOL/TEGDN 38.73/27.19/6.92/24.36/0.36/2.44	1.89	6130
HBX-1	RDX/TNT/AL/WAX	1.72	7310
HBX-3	PBX/TNT/AL/WAX 31/29/35/5	1.82	7310

The shape of the explosive is also an important factor. The typical explosive is spherical in shape; however, by changing the shape, different pressure and energy profiles can be achieved. Huang et al. [11] investigated the effects of changing the explosive shape from spherical to a slender rod with varying degrees of the slenderness ratio. This was achieved by a Multi-Material Arbitrary Lagrangian Eulerian (MM-ALE) method and verified through physical experimentation of varying explosive shapes. They found that the slenderness of the explosive directly affects the resultant pressure field's shape, with the shape becoming more and more nonlinear as the slenderness ratio increases. Additionally, the energy distribution of the slender explosive is similar to that of the spherical explosive; however, the efficacy of the energy is lower. This effect is exacerbated with distance. Overall, the research found that the shape of the explosive affects the pressure but not to such a degree that the load exhibited by the charge changed dramatically [11].

2.3.2 - Analysis via Empirical Equations

The similitude equations, developed by the Naval Ordnance Laboratories (NOL) in the 1950s–1960s, are a series of relationships describing the behavior of shock wave pressure at a given point [4]. These equations are typically used as a form of basic validation for hydrocode for free-field UNDEX. The equations revolve around the use of a decay or time constant defined as the value of time at which a shock wave's rate of decay drastically decreases from exponential decay [2]. The time constant's value changes depending on the type of explosive as shown in Table 2.2 [4]. With these similitude equations, shock wave behavior can be approximated through hydrocode or hand calculations.

Table 2.2. Similitude constants and parameters for various explosives [4].

Explosive	P_m (MPa)		$\Theta/W^{1/3}(ms/kg^{1/3})$		$\frac{I}{W^{\frac{1}{3}}}(kPa \cdot s/kg^{1/3})$		$E/W^{1/3}(m \cdot kPa/kg^{1/3})$		Range of Validity
	K	$\propto$	**K**	$\propto$	**K**	$\propto$	**K**	$\propto$	
TNT	52.4	1.13	0.084	−0.23	5.75	0.89	84.4	2.04	3.4–138
Pentolite	56.5	1.14	0.084	−0.23	5.73	0.91	92.0	2.04	3.4–138
H-6	59.2	1.19	0.088	−0.28	6.58	0.91	115.3	2.08	10.3–138
HBX-1	56.7	1.15	0.083	−0.29	6.42	0.85	106.2	2.00	3.4–60
HBX-1*	56.1	1.37	0.088	−0.36	6.15	0.95	107.2	2.26	60–500
HBX-3	50.3	1.14	0.091	−0.218	6.33	0.90	90.9	2.02	3.4–60
HBX-3*	54.3	1.18	0.091	−0.218 **	6.70	0.80	114.4	1.97	60–350

* Equations for these explosives are based on limited data beyond pressures equaling 130 MPa and so should be used with caution

** Shock wave doesn't act exponentially, but instead has a hump; the similitude equation acts after the hump

All parameters in Table 2.2 follow the form shown in Equation (2.1).

$$Parameter = K\left(\frac{W^{\frac{1}{3}}}{R}\right)^{\propto} \qquad (2.1)$$

where P_m is the peak pressure, θ is the time constant, $\theta/W^{1/3}$ is the reduced time constant, I is the impulse, $I/W^{1/3}$ is the reduced impulse, E is the energy flux density, $E/W^{1/3}$ is the reduced energy flux density, W is the charge weight in kilograms, and R is the slant range in meters. K and $\propto$ are similitude constants that are based on the explosive used and the parameter being examined. It is noteworthy to remember that the equations are only valid within the appropriate ranges of validity and that the equations are based on data developed from beyond 130 MPa. Additionally, the similitude equations fit into the portion of the shockwave that is beyond the hump of the wave as opposed to the entire event. Lastly, I and E are integrated to a time equal to 5θ, representing 5 times the time constant of the pressure wave.

Typically, shock waves display a reasonably replicable behavior in open-field UNDEX when it comes to the pressure-time history. The pressure acts as an exponential function of time for the UNDEX up to a certain time. This decay is approximately equal to 1/e or about 37% in the time of one decay constant. After one decay constant has passed, the pressure decays at a much slower rate [2].

While the peak pressure graph is easily replicable in free-field scenarios, the presence of structures can affect the pressure values in an UNDEX scenario due to rarefaction and reflection waves [2]. Thus, the use of free-field equations is typically used for validation of hydrocodes [4]. For example, Urgessa and Lohner [12] validated results from a computational fluid dynamics code using data obtained from physical testing results of a free-field UNDEX event.

The case of structural equations depends on the type of structures that are being analyzed. As an example, the equations used for analyzing vertical cylinders are not the same as the equations used to analyze dams. However, they are still based on the same concepts of developing from the empirical equations and from underlying physical principles such as the Navier–Stokes equations for fluid behavior. For example, Wang et al. [13] presented extensive formulas and models for the purposes of analyzing vertical cylinders subjected to UNDEX through the similitude equations and other prior known equations.

2.3.3 - Analysis via Numerical Methods/Hydrocodes

According to Mair [14], hydrocodes are computational continuum mechanics tools that simulate the response of both solid and fluid material under such highly dynamic situations that shock wave propagation is a dominant feature. They are designed to model the environment as well as the matter during which dynamic events occur, such as UNDEX. Hydrocodes are built towards specific problems much like any intensive computer code [14]. However, there is a common architecture, methodology, and workflow between hydrocodes from how the meshes interact with materials to how the data of the problem are processed. This difference in methodology is a main form of categorizing hydrocodes in terms of their mesh generation and their treatment of data points.

Among all hydrocodes is an underlying set of processes that generate the required solutions [15]. The basic flow of work in hydrocodes relies on the Newtonian laws of motion, the equation(s) of state, and the constitutive model. These three pillars direct how matter acts in the hydrocode simulation and yield forces and respective responses. These are seen on the mesh generated by the hydrocode, which discretizes the elements present in the simulation [15]. These meshes can be generated in varying ways based on the application and, thus, elements can interact accordingly with the mesh. With the generation of the mesh as well as the element interaction comes two general forms of hydrocode categorization: Lagrangian and Eulerian.

The categorization of Lagrangian and Eulerian falls in how the mesh interacts with the elements of the hydrocode. For Lagrangian, the mesh follows the elements and remains fixed on them for the duration of the simulation [14]. The implication here is that because the mass element is fixed, the mass flux at the boundaries between elements must be calculated. Deformation of the elements (such as material deformation) causes the mesh to distort and create reductions in time steps or breakdowns in problem advancement. For this reason, the mesh tends to respond better to triangular/tetrahedral elements rather than quadrilateral/hexahedral elements due to the former being more forgiving of distortion [14]. This sort of mesh is well suited for solid structures, as the material does not distort as easily as a fluid such as water or air. Other forms of Lagrangian methods include free Lagrangian method (FLM) and total Lagrangian method

(TLM), which affect mesh behavior and individual elements' time steps, respectively [14].

On the other hand, Eulerian meshes are static in the analyses field as opposed to being fixed on the materials. This negates the problem of mesh distortion and time-step variation between cells as well as allowing for observation of bubble pulses in UNDEX. The weakness of a full-Eulerian mesh is that, because the mesh is static while the simulated materials are not, the cells become mixed between different materials and, thus, the physical characteristics inside those cells change. Additionally, the presence of solids in a Eulerian mesh creates a need for the solid structure to be defined in the mesh and, thus, have precise zoning for the solid–fluid interface [14]. Eulerian meshes are best used for fluids in meshes.

The categorization of Lagrangian and Eulerian, however, is not exclusive. A combination of the techniques used in both types of meshes can be used in both Combined Lagrangian-Eulerian (CLE) and Arbitrary Lagrangian-Eulerian (ALE) methods. CLE splits the meshes based on the materials analyzed with Lagrangian representing solids and Eulerian representing fluids. The interface between the two meshes is handled by a coupling mechanism that either develops its own elements or incorporates Lagrangian elements into the Eulerian meshes. This method has clear uses in mixed-state problems such as analyzing airplane foils' impact from air flow or UNDEX effects on structures [14]. However, the method is weak to situations that create a rift in the Eulerian elements with the Lagrangian structures. The Lagrangian elements split the Eulerian elements apart at the cell, causing computational issues [14]. Despite this, CLE is still a popular method of simulation for UNDEX events.

The alternative to CLE is ALE, which is based on the concept of incorporating Lagrangian algorithms into a Eulerian mesh. This is done by analyzing the mesh at every time step by determining Lagrangian motion and if the mesh needs to be rezoned or not, thus combining the Eulerian and Lagrangian mesh styles. This algorithm can be performed with varying degrees of intensity by either only focusing on one material or by focusing on multiple materials with regards to mesh deformation [14]. This creates a difference of stability and computational speed. ALE is better suited for structure-fluid coupling due to the interface between the two being Lagrangian in nature rather than Eulerian; however, it can still fail in the same manner due to a 'pinching' nature of the Lagrangian elements when coupling the fluid-structure regions through matching element nodes [14].

Separate from the Lagrangian-Eulerian categorization is the Smoothed Particle Hydrodynamics (SPH) method. This method revolves around assigning each particle present in the mesh physical characteristics as opposed to the elements [15]. These particles are then tracked throughout the simulation and analyzed based on the forces exerted upon them. This is a form of Lagrangian analysis due to following the individual particles as opposed to the static Eulerian mesh; however, the elements in this mesh are not considered. This method is fairly simplistic due to only following the particles; however, it does run into complications when tackling complex boundary conditions and large density disparities. Despite these issues, SPH is a satisfactory algorithm for fluid problems with low densities and inflow or outflow conditions as well as problems with self-gravity such as solar systems.

Liu et al. [16] presented a smoothed particle hydrodynamics method to simulate UNDEX problems. Their work provides extensive details on the numerical procedures, including the use of artificial viscosity, smoothing length evolution, treatment of solid boundary, material interface consideration, and the Leapfrog time integration scheme. They showed the effectiveness of the SPH method using three case studies: one-dimensional TNT slab detonation, underwater explosion in free space, and underwater explosion in a confined chamber.

Afrasiabi and Mohammadi [17] presented a newly developed stabilized SPH method by implementing a velocity field smoothing technique. They also incorporated an adaptive smoothing length and the penalty force exertion scheme. The stabilized SPH method was applied to analyze spatial and temporal variations of density, pressure, internal energy, and velocity in UNDEX in addition to bubble formation and evolution.

Zhang et al. [18] used SPH to simulate a shaped-charge detonation, formation of a metal jet, and penetration of a steel plate in UNDEX. The SPH method was shown to be effective because the numerical simulation results were all in good agreement with experimental results.

2.4 - Structures Encountered in UNDEX Analysis

Due to the nature of threats that UNDEX can present, the types of structures that can be affected are numerous. In this subsection, the following structures are discussed:

1. Ships;
2. Concrete dams;
3. Reinforced concrete (RC) slabs;
4. Reinforced concrete columns;
5. Miscellaneous structures.

2.4.1 - Ships

Ships are a popular subject for analysis in UNDEX events. The prevalence of naval military conflict as well as accidents creates a need for inspections on ships' abilities to withstand UNDEX. As noted before, it is unwieldy to do physical testing on a full-sized ship, so smaller models are typically used as study subjects and references for hydrocode. For example, Ming et al. [6] used air-backed steel plating to examine UNDEX effects on a ship's hull. The tests generated a series of damage profiles of a ship subjected to UNDEX effects, mainly characteristics of bulging, discing, and petaling. Steel cylinders is another option for analyzing steel behavior or as a rudimentary model of an entire ship's body, more specifically submarines. As an example, Gannon [19] used this approach for hydrocode verification on submarine analysis. These models are then used for verification of hydrocode models and have been found to be reliable tools for analyzing ship response. The important note in comparing the analysis of ships to civil infrastructure such as concrete structures is that the behavior of steel is linear or plastic unlike concrete [19]. So, while the methodology of the experimentation to data collecting is the same, the specific equations and relationships will differ considerably. Despite that this review chapter's focus is on the response of concrete structures to UNDEX, the prevalence of ship analysis is noteworthy.

2.4.2 - Concrete Dams

Among the concrete structures analyzed for UNDEX in literature, dams are among the most common due to the verification of their safety for terrorist attacks and structural failures. While dams suffer from the same logistical issues as ships, the solution of creating scaled-down models involves the usage of centrifugal modeling, as described in a previous section. Additionally, the nonlinear behavior of concrete compared to steel creates a need for a different computational model through differing hydrocodes and equations of state.

Vanadit-Ellis and Davis [9] verified the centrifugal laws for dams through the use of practical models and hydrocodes. The model dams were made in-house through a basic concrete pour over a wooden mold and steel base plating. These models were then subjected to hardness tests to verify strength, then subjected to UNDEX yielding. The concrete can fail in three ways: material failure due to crushing/spalling, localized failure due to tensile/shear stresses, and structural failure due to tensile bending stresses.

It was found that these failure modes had different intensities depending on the stand-off distance of the explosion as well as the thickness of the dam [9]. For thick panels, detonations nearby the panel surface can cause the concrete to fail due to crushing and back-face spalling due to coupled stresses moving directly through the concrete. For thinner panels and slightly greater stand-offs, the panels fail in a “punching shear” mode, which is localized for relatively small charges. For still greater stand-offs, the pressures applied to the panel are too low to cause either of the first two modes of failure but are distributed over an area wide enough for the total load to break the panel in a beam-type (or cantilever) structural bending failure. It was found that the centrifugal laws accurately depicted the structural response of a concrete dam and that the experimental data provided can be of use for further research purposes as hydrocode validation [9].

Ren et al. [20] studied the numerical verification of hydrocode based on dam analysis. This verification was undertaken by comparing Vanadit-Ellis and Davis’ physical experiment and Ren’s hydrocode. Ren’s code differentiates itself through modeling the dam completely as opposed to analyzing the dam in stages or ‘slices’. This was achieved using a 3D full coupling model developed through ABAQUS, allowing for the full 3D damage profiles of the dam to be obtained, which cannot be done with the slice method. This model was then subjected to simulated UNDEX and analyzed using a rate-dependency damage-plasticity model that then generated the damage and failure data. It was found that this series of methods accurately represented the same data that were physically determined by Vanadit-Ellis and Davis. Ren et al. found that dams affected by UNDEX suffer mainly tensile damage, which is concentrated in the upstream surface of the dam as well as the dam head. This damage decreased with increased stand-off distance, but also increased the number of abnormal data points in the breach area. Ren recommended the countermeasures of increased tensile strength as well as reinforcement of the dam head, upstream surface, and the inside part of the dam [20].

Due to the nonlinear nature of concrete, analyzing it within hydrocode can pose problems due to simulations failing for a variety of reasons such as suboptimal damage models or oversimplification. The development of a concrete damage plasticity (CDP) model could solve those problems through accurately modeling the concrete throughout various states such as compression, tension, and other effects. This model was put forward by Moradloo et al. [21], who designed a set of behaviors, parameters, damage and stiffness recovery algorithms, and governing equations to accurately depict concrete throughout the UNDEX event. This model was verified through testing an UNDEX event on an aluminum cylinder similar to the experiment performed by Kwon and Fox [43] examined by Evans [4]. The model was then used to model an arch concrete dam that was then subjected to a series of UNDEX simulations. It was found that the CDP model was valid with the simulations put forward with the analysis of the damage profiles showing similar behaviors from previous dam research such as increased damage with increased stand-off distance. Additionally, charge depth increased the damage of the dam due to the bubble pulse not venting towards the surface and instead the energy imparting onto the reservoir face [21].

2.4.3 - Reinforced Concrete (RC) Slabs

RC slabs are used as load-bearing members for many marine structures such as docks, piers, and factories. Thus, an examination on their UNDEX resistance should be examined. Hai et al. [22] studied the damage profiles of air-backed RC slabs. To develop proper data for these profiles, physical experimentation was done by subjecting an RC slab that was air-backed on one side and submerged in water on the other to an UNDEX event. This experiment yielded pressure-time and strain-time histories that were replicable in LS-DYNA through a hydrocode simulation. This hydrocode simulation was then used to conduct a more thorough investigation into the UNDEX event and its effects on the slab. It was found that much of the displacement of the slab occurred during the bubble pulse timing and not due to the initial shock wave. Additionally, increased stand-off distance exacerbated the damage on the RC slab with the concrete nearest to the charge location being crushed during the shock wave and having cracks propagate throughout the rest of the UNDEX event [22]. Hai et al. also developed two different computational models for capturing the failure of concrete. One model was based on the concrete damage-plasticity model (CDPM). This model allows for the concrete to be accurately simulated through multi-axial and rate-dependent loadings. This is done through a series of stress-strain equations and classical damage parameter equations. The other was based on the bond-based peridynamic (PD) theory that replaces the partial differential equations that are the typical standard for modeling concrete with integral equations. The PD model uses a series of equations relating the density of body, displacement vector, the peridynamic horizon, body force density, and the pairwise bond force density to form its material defining equations [22]. The PD model came from a need for a model that can accurately model cracks, fractures, and other discontinuities that could not be modeled by classic continuum mechanics. The integral equations remain valid throughout the failure process of the concrete and thus are a good choice for modeling the RC slabs [22]. Both of these models were found to be sufficient for modeling concrete as it undergoes the UNDEX event.

Zhao et al. [23] conducted a series of experiments regarding proper modeling of RC slabs. This comparison was conducted by analyzing the damage profiles of each method of an RC slab subjected to both UNDEX and air explosions (AIREX) [23]. This was done through testing the hydrocode formulations of CEL, SPH, and coupled finite element method-SPH (FEM-SPH). The benefit of FEM-SPH over standard SPH is that the FEM nodes can model the smaller deformations while the SPH particles model the larger deformations as well as the model explosion [23]. Both sets of nodes and particles are linked to each other and exchange information, allowing them to complete the same calculations as standard SPH at a faster time. Due to this trait, it was found that the FEM-SPH method is best at modeling as it is faster than SPH and more accurate than the CEL method, which was found to be unable to properly model the steel reinforcements inside the tested RC slab [23]. The results of the damage profile as well as the analysis of the RC slab's behavior during the UNDEX event were investigated. It was found that under UNDEX, the main failures were through spalling and punching failures with areas of the slab, notably the top surface and the lower layer steel reinforcement, which suffered heavy damage and complete failure [23].

2.4.4 - Reinforced Concrete/Bridge Columns

RC columns, like RC slabs, are used as load-bearing members of structures and thus can be vulnerable to blast loadings. While the effects of air blasts on RC columns are well-known, UNDEX effects are less documented. Yang et al. [24] analyzed RC columns under both of these effects. For the UNDEX analysis, a fully coupled 3D Lagrangian and Eulerian numerical method was used to simulate its effects on RC columns with varying cross-sections. This numerical model was validated through the use of physical experimentation conducted on an RC column with a square cross-section of 400 mm by 400 mm [24].

The numerical CLE model was found to be accurate through a comparison of the damage profiles and dynamic response of both the numerical and experimental methods. With the numerical model verified, analysis of the different RC columns was conducted with a focus on cross-section shapes. It was found that circular cross-sections worked best for anti-knock purposes due to the diffraction of the shock waves and the compounding of stress waves in the square RC column from the corners of the column. Furthermore, Yang et al. conducted a parametric study on anti-knock measures and their effectiveness. This was done by examining varying concrete properties, reinforcement spacings, and reinforcement thickness. It was found that the use of ultra-performance concrete works best for damage control with decreasing the reinforcement spacing with introducing more reinforcements to the column being the next best measure [24].

Zhuang et al. [25] studied the dynamic response and damage model of circular RC columns through physical experimentation of UNDEX effects on a scaled-down RC circular column and a steel column. The main consideration for the physical experimentation was the load distribution; thus, the data for pressure, acceleration, strain, and displacement were used. The RC column and steel column were subjected to charges with varying masses between 0.05 and 0.8 kg depending on the experimental parameters and purpose set. Due to the expectation that the RC column would deform under UNDEX while the steel column would not, the displacement, acceleration, and strain sensors were placed on the RC column while the pressure sensors were placed on the steel column

[25]. These columns were then subjected to UNDEX and the data sets for displacement, acceleration, strain, and pressure were recorded.

The physical data suggest that the shock wave loading refracts due to the round surface of the column with the diffracted pressure being less than that of the shock pressure. This observation is affected by the explosive quantity, proportional stand-off distance, and the detonation depth. Additionally, the bubble pulse is severely hampered due to the proximity of the air–water surface, which causes the energy caused by the bubble pulse to be dispersed upwards into the air as opposed to into the column. This causes low explosive quantities to generate smaller bubble pulses and thus less energy, while higher explosive quantities create a larger bubble pulse that vents to the surface and thus does not create a fully realized bubble pulse. Lastly, Zhuang et al. drew several relationships for predicting shock wave load including the neglecting free surface effects due to explosive quantity and detonation depth, the inverse relation of the diffraction coefficient (equal to the ratio of shock wave peak pressure and diffracted shock wave pressure) with proportional stand-off distance following the least square method, and the calculation of net peak pressure of the shock wave through the reflected and diffracted shock wave peak pressures [25].

With the physical data, a series of parametric studies was performed with an analysis on the effects of explosive quantity, stand-off distance, detonation depth, and proportional stand-off distance on the damage profiles of the columns. The damage and displacement of the RC column was increased with increased explosive quantity. It was found that for explosive quantities, a weight of 0.2 kg of TNT caused the existence of two separate pressure peaks in the pressure-time graph (with the second peak being caused by bubble pulse), while any amount above that resulted in only the shock wave being seen. This correlates with the observations mentioned earlier. For increasing stand-off distance, the shock wave load decreased dramatically with the reflected and diffracted shock wave loads acting similarly. With regard to the detonation depth, the larger detonation depths resulted in higher bubble pulse effects with an observed critical value of non-dimensional detonation depth (ratio of detonation depth and cube root of charge mass) of 1.71 below which no bubble pulsation effects were observed. Additionally, once the detonation depth reached a value below 0.34 m, it was considered a non-factor with regards to damage.

The damage profiles observed indicated failure modes of bending, bending shear, and punching. These failure modes take different priorities depending on the situation. Bending failures typically took precedence in situations of small charge masses and large stand-off distances. Shearing failure occurs near the ends of the columns with an increase of charge mass and decrease in stand-off distance. Finally, punching failure occurs after the stand-off distance is within a certain threshold [25].

Further research into damage effects, and specifically safety distances, has been conducted by Loomis [8] for the purposes of bridge safety from UNDEX. This study was conducted through a CLE numerical model developed through DYSMAS that includes sand elements as well as the titular air, water, explosive, and concrete elements. This model is a representation of the foundations of a concrete bridge and thus would accurately depict UNDEX effects. The model also generates a damage parameter for each element that determines the damage state of that element. It was found that the damage parameter will rise as long as the simulations are able to run due to concrete's tendency to degrade from crumbling past the UNDEX effect [8]. This is critical as this allows for long-term damage effects to be simulated. Through the simulation of this model, two parametric studies were conducted: a depth study and a sensitivity study. For the depth study, the depth and stand-off distances of the explosive charge (50 kg of TNT) were varied from shallow to deep depths and near to far stand-off distances. Damage was measured through measuring stress of each foundation element during and after the UNDEX event. It was determined that the configuration of intermediate depth and nearby stand-off distance creates the most damage. This is due in part to the weakness of the foundation corners, which causes more load to be imparted onto the top and sides of the foundation. The nearby stand-off distance ensures that the UNDEX shock wave is not excessively dissipated by the water before reaching the foundation. Additionally, the deep depth caused relatively little damage due to the shock wave, only hitting the sides of the foundation and the deeper depth, thus causing more energy to be expended overcoming the higher hydrostatic pressure [8].

The sensitivity study was split into three sub-categories: the load sensitivity, the reinforcement orientation sensitivity, and the reinforcement volume fraction sensitivity.

These were done in order to develop the parameters for an accurate, high-fidelity model. The load sensitivity was conducted through applying five different loads onto the foundation to analyze the change in the damage parameter. It was found that the damage parameter did increase with increased load but to such an extent that it was considered insensitive to the load changes and, thus, the models were not changed with varying load sizes. The reinforcement orientation study found that the z-direction rebar placed perpendicular to the shockwave was the most critical element in the reinforcement assembly and should be depicted most accurately within the model. Lastly, the reinforcement volume fraction was analyzed. It was found that as the reinforcement volume fraction increased, the damage parameter decreased at varying rates [8].

A practical example of a load-bearing column would be an RC pile, which is typically used to support structures over water such as docks or wharfs. In the case of UNDEX targeting these piles, the structural response would be similar to that of a typical RC column under similar conditions. Yan et al. [26] conducted research on the RC pile with an analysis on the effects of various parameter alterations on the safety distance of the UNDEX. This was done by physical and numerical modeling. The physical model was an RC concrete column submerged partially with water and subjected to near-field UNDEX. The numerical model consisted of a CLE model designed with AUTODYN that incorporates the standard elements of air, water, explosives, and concrete. The model was verified through the comparison of the final displacements and damage of both the physical and numerical models undergoing the same UNDEX event. It was found that the models correlated, and the numerical model was satisfactory.

The numerical model was then used to conduct a series of studies regarding the damage and failure assessments of the RC pile as well as certain effects on the safety distance of the piles. The damage and failure assessments of the RC piles found that with near-field UNDEX, local failure would take precedence and gradually give way to bending then shearing failure as the stand-off distance was increased. Additionally, the damage on the concrete increases with increased depth with more damage being shown at the bottom end of the pile. It was also found that most of the damage was caused through the bubble pulsation event, not the shock wave. Through this analysis, an assessment method for the damage called the damage index was used to perform the damage analysis, which also found that increased stand-off distance decreased damage. With the results of the damage and failure analyses, a series of parametric studies were conducted with a focus on the safety distance. The parameters examined were the charge quantity, blasting depth, steel hooping ratio, concrete strength, and longitudinal reinforcement ratio. It was found that the safety distance shared a direct relationship with the charge quantity while holding an inverse relationship with the steel hooping ratio, concrete strength, and longitudinal reinforcement ratio [26]. The relationship with the safety distance and the blasting depth initially starts as inverse but becomes direct as the depth increases. With these parameters, a safety distance formula was proposed.

2.4.5 - Other Structures

Wang et al. [12] focused on the development of a substructure method for analyzing the transient response of cylinders undergoing UNDEX shock waves. This was done through a numerical model that was verified via a comparison of the numerical response and the results of the Liaw and Chopra [27]. The numerical model was developed through AUTODYN and mathematical formulation. It was found that there are three sub-pressure waves that occur in UNDEX that affect the cylinders: the incident shock wave pressure, the scattered wave pressure, and the radiation pressure from the cylinder displacement during the UNDEX event. It was also found that the transient response can be reduced through the stand-off distance of the charge and the radiation wave, with the effects being more apparent for slender cylinders [12].

Explosive effects on underground structures such as tunnels are also a concern. These explosive effects can be tested physically through the use of a centrifuge similar to the Vanadit-Ellis/Davis experiments. De et al. [10] developed a series of experiments involving physical and numerical simulation of a tunnel covered in soil that was then covered in water [10]. The physical simulation was performed with the use of a geotechnical centrifuge, which allowed the physical experiment to make use of the centrifugal scaling laws similar to those used in the dam experiments by Vanadit-Ellis and Davis and Ren [9]. Data collection on the physical model included a series of strain gauges and pore pressure transducers. The resultant data were then used to develop a model in ANSYS using the CLE method. Multiple parametric studies were conducted to develop relationships between the various materials present in the simulation. It was found that the depth of the water simultaneously increased the total pressure imparted by the explosive charge on the tunnel and created higher strain within the soil [10].

2.5 - Summary of Literature Review

This chapter presented a state-of-the-art review of the research on UNDEX effects on structures with a particular focus on concrete structures. The fundamentals of the UNDEX event and the analysis models are presented. The UNDEX event is a multi-step process with each step being impactful to the entire scope of the event. Physical experimentation is difficult due to the nature of UNDEX; however, proper facilitation and mathematical scaling laws allow for physical models to be fabricated. Variations in computer algorithms and hydrocodes have allowed these events to be accurately portrayed in a variety of cases and successfully resemble physical experiments. Steel and concrete structures are the standard subjects of analysis with the behavior of both varying due to their physical properties. Several concrete structures, including dams, columns, and slabs subjected to UNDEX are discussed with brief descriptions provided for the studies presented on ships and tunnels.

Further directions for research would include the exploration of UNDEX effects on wooden structures, further testing on anti-blast measures such as high-performance composite fibers, and testing of explosive effects in partial submerged scenarios. Additionally, research can also be expanded in the fields on frames and trusses such as on pedestrian bridges or other infrastructure. In terms of analytical methods, uncoupled analysis was not mentioned within the existing literature and so is a source of further study. For the purposes of this thesis, the work done on the analysis of RC columns holds special focus. This is due to the similar subject of research and the ability to use the work presented for verification studies in the subsequent chapters. That being said, this review is comprehensive of the current research done in the study of UNDEX and thus should provide a good resource for future researchers to not only get an overview of the topic but also to provide additional readings on the subject.

CHAPTER THREE

This chapter discusses the initial verification of computational methods for the use of structural modeling. This involves basic modeling in ABAQUS, a 3-D modeling program with a focus on FEA, and earlier validations. Two documents from the literature review align closely with this thesis and thus are used as guidelines for modeling RC columns. While these models are not the main focus of the thesis, they were used to reinforce confidence in using ABAQUS.

3.1 - Validation Studies for Preliminary Dynamic Loads

The initial papers examined for this research were Yang [24] and Zhuang [25]. While focusing on varying details of structural response, both authors wrote extensively on the effects of blast loading on concrete structures, specifically concrete columns. Yang [24] focused on the effects of preventative measures such as cross-section shape and reducing spacing between reinforcements. Zhuang [25] focused more on the mechanics of the loading, examining the main pressure from the blast, the reflection wave, and the bubble pulse pressures from the submerged gasses left from the explosion process.

Before proceeding with investigating the dynamic response of RC columns subjected to blast, dynamic analysis and verification were conducted using a finite element software. Column configurations and geometries from Yang and Zhuang's experiments were analyzed with ABAQUS CAE, an FEA program built to analyze static and dynamic loading conditions on structures. Both Yang and Zhuang detailed the experiments they conducted with pressure profiles, column models, and expected displacements. Additionally, conclusions drawn by both authors can be used as a preliminary form of validation for the sensitivity studies presented later in this thesis. For instance, Yang concluded that the cross-section of the column has a major effect on the column's ability to withstand blast with circular columns having less displacement than square columns. Zhuang concluded the effects of varying parameters for UNDEX for RC columns including explosive stand-off distance, detonation depth, explosive quantity, among others.

The initial work on modeling with ABAQUS was focused on verifying its validity through dynamic analysis. This work will involve the examination of a column subjected to varying boundary and load conditions applied to one face of the column. A square column made of A36 steel was modeled and subjected to a uniform distributed load of 3MPa and a triangularly distributed load of 3MPa at its maximum placed at the supported end. Steel was used initially due to its homogeneous nature, making it suitable for comparison between software and hand calculations. The column is modeled with a square cross-section with side lengths of 0.4m and a height of 3.85m. The column was modeled to be fixed at one end and free on the other as shown in Figure 3.1.

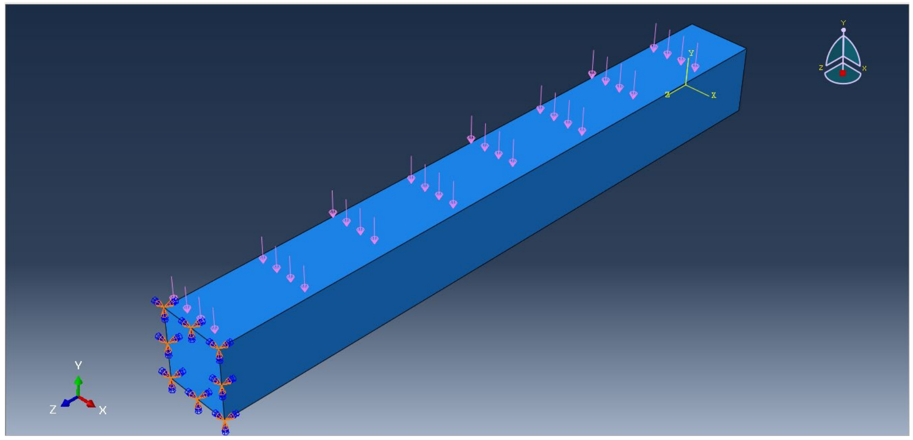

Figure 3.1. Loading and Boundary Conditions for Basic Dynamic Load Study Validation for Rectangular Pulse Loads

The displacement of the column's free end obtained from ABAQUS was compared to hand calculations for both the uniformly distributed loads (UDL) and triangular load applied with the maximum pressure placed at the fixed end, respectively computed with Equation 3.1 and 3.2.

$$\Delta = \frac{wx^2}{24EI}(x^2 - 4Lx + 6L^2) \tag{3.1}$$

$$\Delta = \frac{wx^2}{120EIL}(10L^3 - 10L^2x + 5Lx^2 - x^3) \tag{3.2}$$

Where Δ is the displacement, w is the maximum load, E is the modulus of elasticity, I is the moment of inertia, x is the height variable with height of 0 being placed at the fixed end, and L is the full height of the column.

It was found that the results correlated with a deviation of less than 2% for the free end of the column for the uniformly distributed load case as shown in Figure 3.2 and the triangularly distributed load as shown in Figure 3.3. Additionally, the maximum principal stress of the column at the supported end was calculated with Equation 3.3:

$$\sigma = \frac{Mc}{I} \tag{3.3}$$

Where σ is the von Mises stress, M is the bending moment, C is distance from the the neutral axis to the external fiber of the column, and I is the moment of inertia.

It was found that for the UDL and triangular loading cases, the error was 0.16% and 0.07% respectively for the outmost fiber of the column. This, along with the displacement studies, verifies the validity of the ABAQUS outputs.

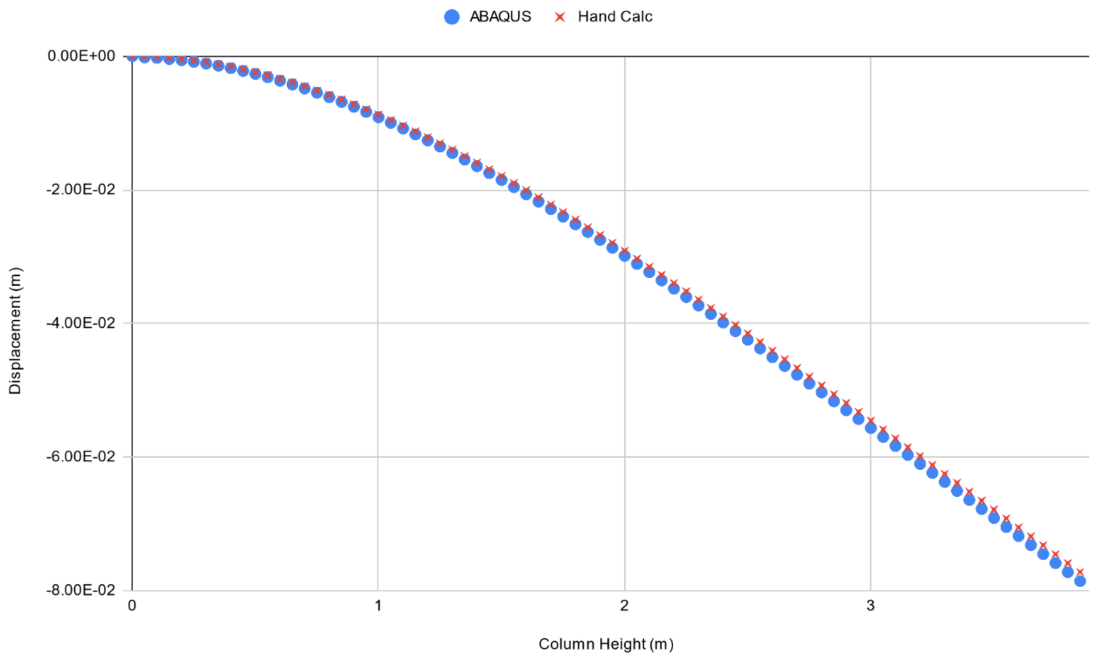

Figure 3.2. Deflection Verification Study of a Steel Column with Fixed and Free End under Uniformly Distributed Rectangular Pulse Load of 3MPa

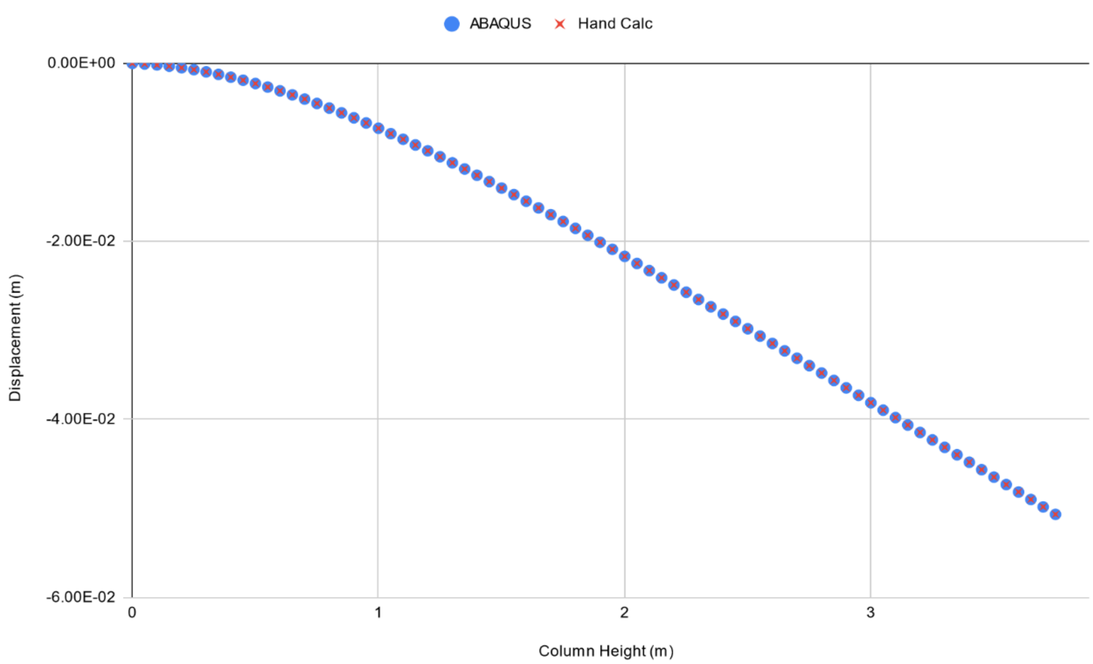

Figure 3.3. Deflection Verification Study of a Steel Column with Free and Fixed ends under Triangularly Distributed Rectangular Pulse Load of 3MPa

Additionally, a column with the same dimensions but with a different boundary condition was examined. The free end was replaced by a roller end and its displacements were examined under the same 3MPa UDL condition. The displacement of the column was calculated via Equation 3.4.

$$v = \frac{w_0 x}{48EI}(L^3 - 3Lx^2 + 2x^3) \tag{3.4}$$

Where v is the displacement, w_0 is the maximum load, E is the modulus of elasticity, I is the moment of inertia, x is the height variable with height of 0 being at the fixed end, and L is the full height of the column.

It was found that the displacement of the ABAQUS model was conservative in its estimate when compared to the hand calculation as shown in Figure 3.4, but it represents the physical model within an acceptable range of error. Next, a model with the triangular load and a polynomial loading nicknamed ‘Blast’ was used to simulate the anticipated loading from an explosive placed near the base (fixed end) of the column at 0.05m height. This profile can be seen in Figure 3.5.

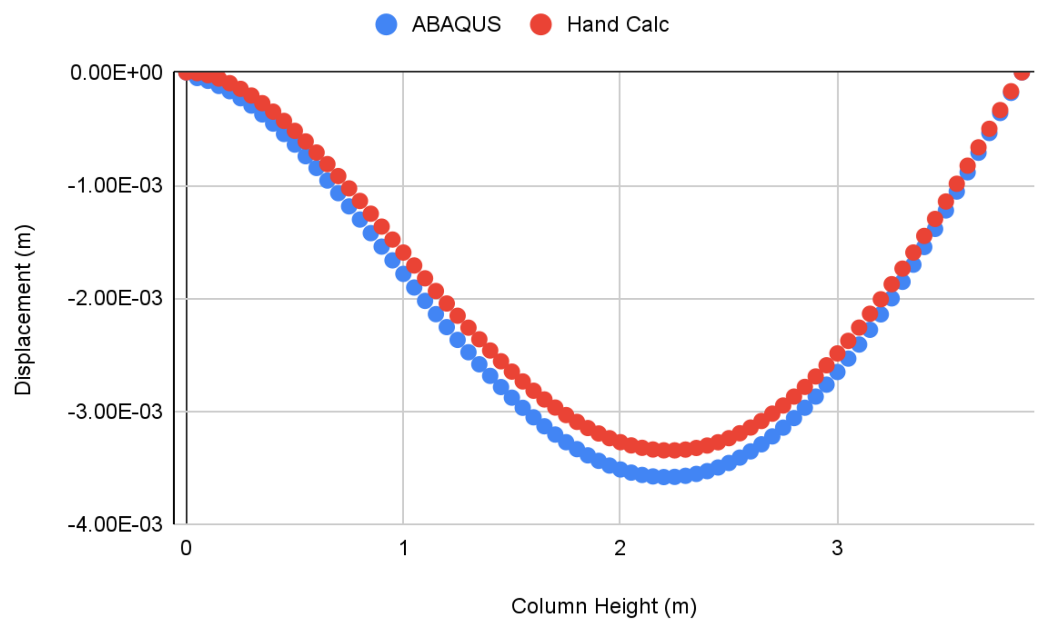

Figure 3.4. Deflection Verification Study of a Steel Column with Fixed end and Roller end under Static UDL of 3MPa

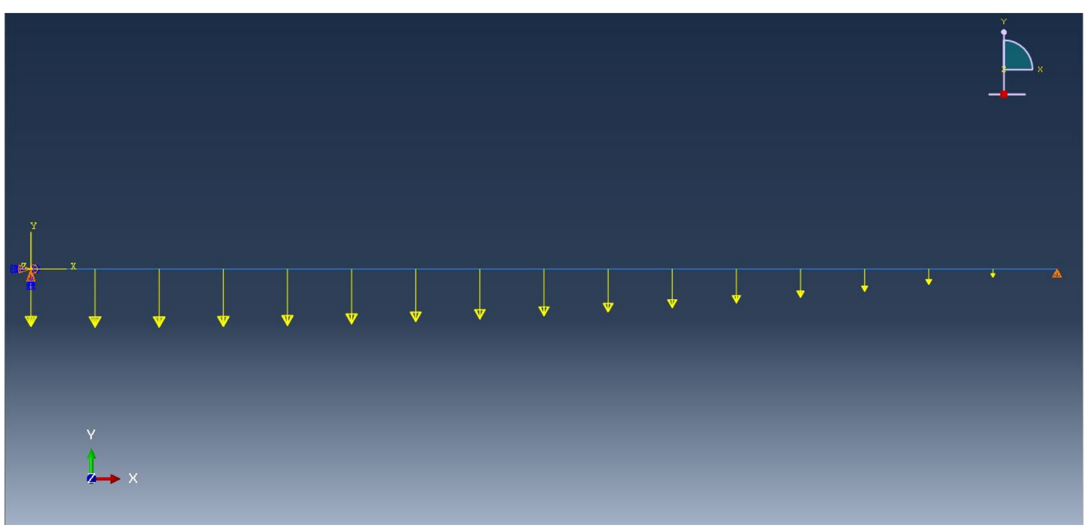

Figure 3.5. Polynomial 'Blast' Profile

This verification study is meant to get a general estimate of the column's response to differing loadings with each successive loading getting closer to the anticipated blast loading. As shown in Figure 3.6, the Blast profile had a larger impact on the column's displacement compared to both the UDL and triangular loading case, implying that the distribution of the load is significant to the profile given the maximum loading on all three cases is the same.

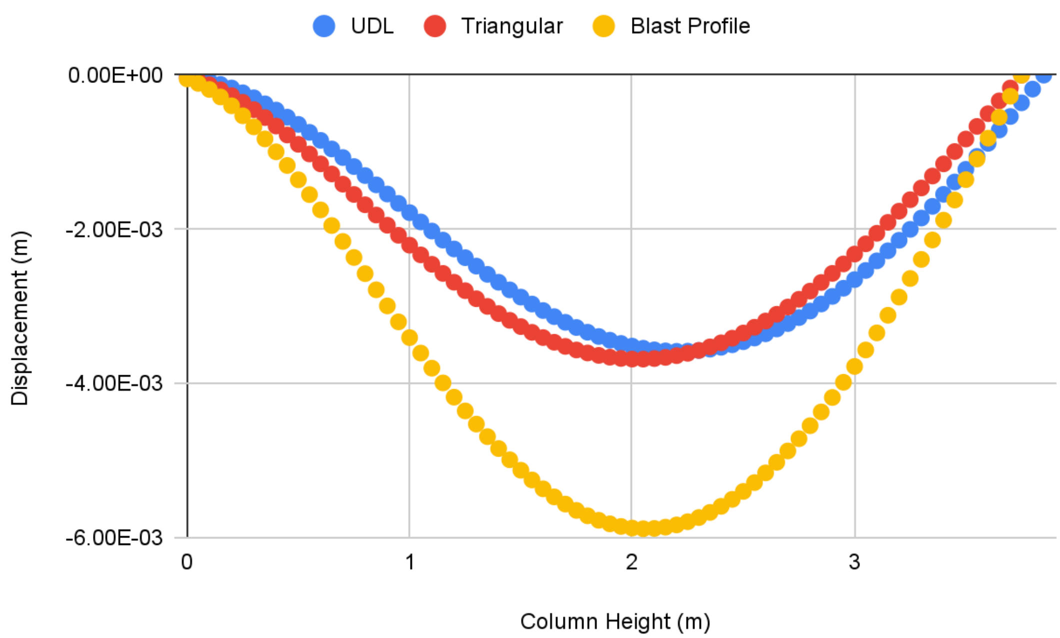

Figure 3.6. Deflection Verification Study of a Steel Column with Fixed end and Roller end under varying 3MPa loadings

Following the dynamic analysis, a series of models were developed to determine the best form of modeling within ABAQUS for the UNDEX scenarios. Firstly, the performance of dynamic analysis was investigated. This is achieved through applying an amplitude to the load applied on the models throughout a timespan, effectively creating a dynamic load. This was first tested with linearly decaying loads spanning over 0.0003s and 0.05s. The loads created were at time-start equal to 3MPa UDL, similar to the load used in the static case, which then decayed to 0 at the end of its lifespan. These loads were applied to the same fixed-end/roller-end steel column. Displacement profiles taken at 1s were recorded for the dynamic cases and juxtaposed to the static displacement profile. As shown in Figure 3.7, the displacement profiles of the dynamic cases are less intense than the static case which is to be expected due to the lower load times.

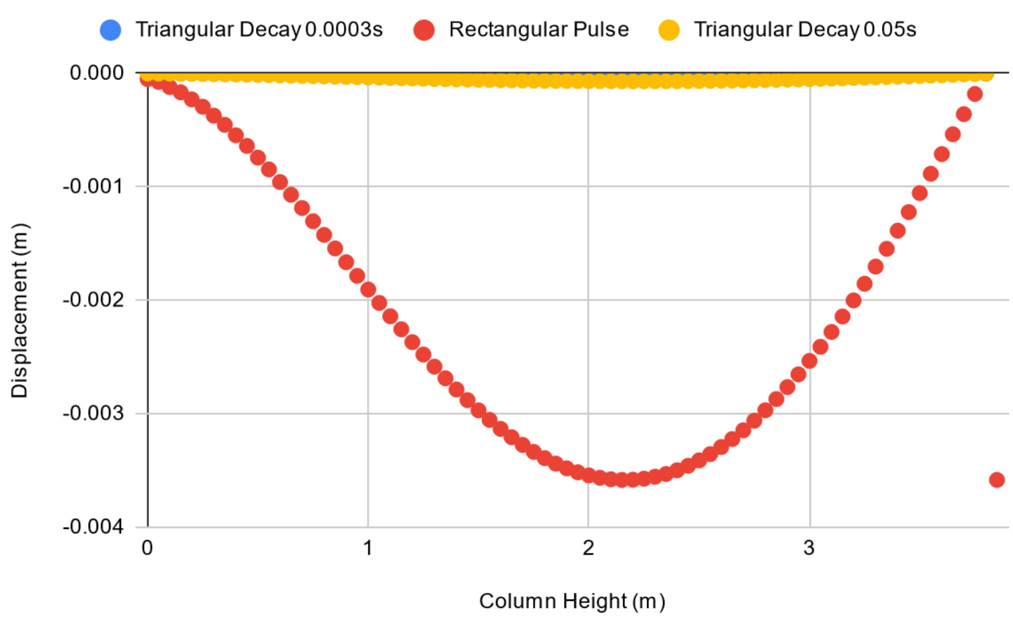

Figure 3.7. Displacement study of a Steel Column with Fixed-End and Roller-End subjected to Dynamic Loading of 3MPa UDL

3.2 - Development of ABAQUS Models for RC Columns

Once the fundamentals of analysis of static and dynamic analysis were well-understood, other forms of analysis such as CONWEP (conventional weapons effects blast loading model) were analyzed. CONWEP is an analysis model based on equations taken from "Design and Analysis of Hardened Structures to Conventional Weapons Effects" [28] which describes structural effects from conventional weapons on varying structures. This includes effects of air and surface blast; however, it does not include effects of UNDEX. For this reason, CONWEP was not considered a good analytical tool for this thesis and merely used for initial exploration.

The inclusion of reinforcements within the column was also examined. This comes in the form of additional entities in the model creation that are arranged in the final assembly. Given the creation of reinforcements, an RC model resembling the model used in Yang's studies was created. This column has side lengths of 0.4m, a height of 3.7m, and reinforcements made from A36 steel. There are a total of 60 stirrups, each with a radius of 4mm and 4 longitudinal reinforcement bars with radii of 6mm placed at a cover distance of 34mm. Six stirrups at the top and bottom of the column had a distance of 100mm from each other with the rest having a distance of 150mm from each other. Figure 3.6 shows the reinforcement for the square column model. Ultimately, the reinforcement is expected to increase the resistance of the column compared to a non-reinforced column.

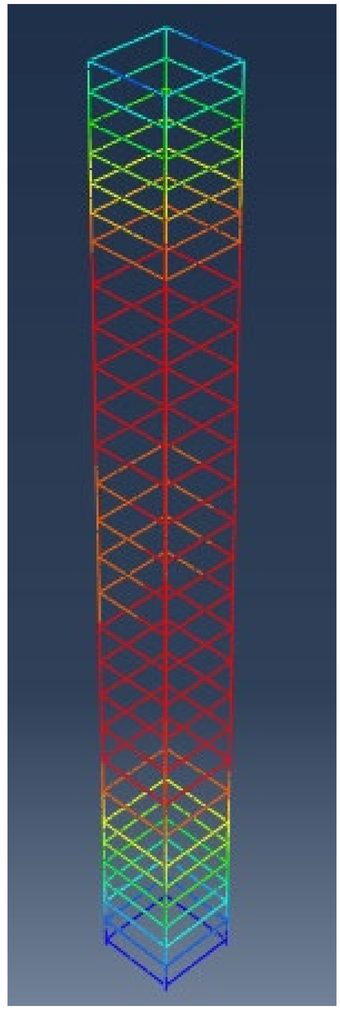

Figure 3.8. Reinforcement of ABAQUS 'Yang' Column

The integration of material modeling in the ABAQUS model was also considered. While the previous models took advantage of basic material modeling such as modulus of elasticity and density, ABAQUS allows for advanced material models to be implemented. For instance, damping becomes a consideration. ABAQUS employs the use of Rayleigh damping which considers damping effects from mass and stiffness effects. This damping is typically used to supplement a model that has no external form of damping such as shock absorbers [29]. The Rayleigh damping equation considers two separate factors: α and β. These factors are associated with the mass proportional damping and the stiffness-proportional damping respectively. Given these factors, the damping equation for Rayleigh damping resembles that of Equation 3.5:

$$\xi_i = \frac{\alpha}{2\omega_i} + \frac{\beta\omega_i}{2} \tag{3.5}$$

Where ξ_i is the fraction of critical damping, w_i is the natural frequency of the column, α is the Rayleigh damping coefficient for mass-proportional damping, and β is the Rayleigh damping coefficient for stiffness-proportional damping.

Given Equation 3.5, it can be seen that α controls the lower frequencies of the damping while β controls the upper frequencies. The relative effects of mass-proportional effects compared to stiffness-proportional effects are unknown within the materials, so for simplicity of this verification study they are assumed to be equal; ie. $\alpha = \beta$. With this assumption made, studies were conducted to examine the difference between common damping ratios. Figure 3.9 depicts displacement profiles of the earlier RC column model subjected to a UDL with a decay matching that of the sample blast data. This blast data can be seen in Figure 3.10. As shown, the displacements decrease between the undamped case and the 2% damped case and less so between the 2% case and the 3% case. This is to be expected given diminishing returns between damping cases.

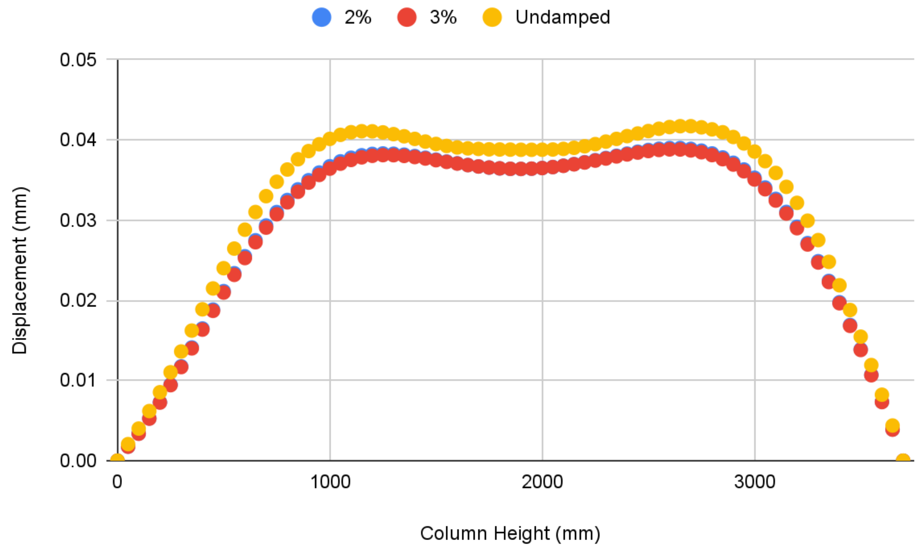

Figure 3.9. Displacement study of a RC Column with Fixed-End and Roller-End subjected to Static and Dynamic Loading of 3MPa UDL

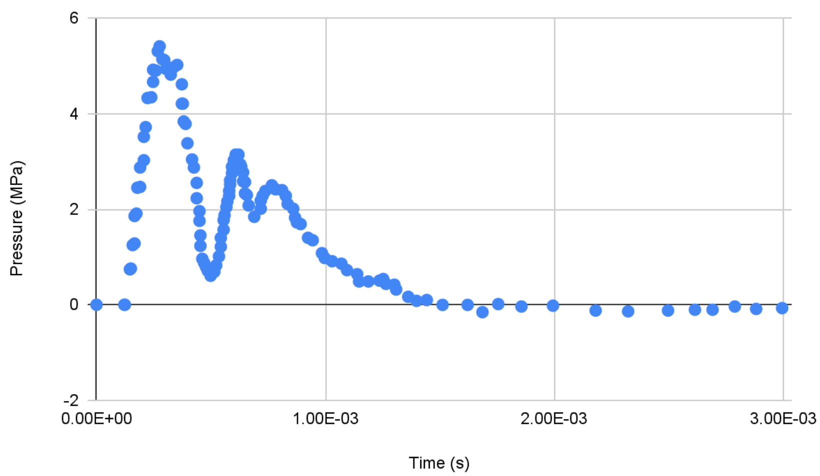

Figure 3.10. Blast Decay Data used for Damped Displacement Study seen in Figure 3.9

ABAQUS also offers structural and composite damping. Structural damping is used to model external mechanical dampers and is not relevant to this mode. Composite damping is used for each material present in the ABAQUS assembly which is then calculated to create the critical damping fraction. While this could be used within the RC model given the two different materials present, it is not known to what extent the concrete dampens the structural response compared to the reinforcement steel and hence it is not used. Additionally, damping within a blast scenario is generally ignored due to the speed at which pressure dissipates during the examination period. Thus, damping was not used for the remainder of the studies conducted.

For the use of materials that are not homogenous such as concrete, more specialized models can be created. In the case of concrete, the concrete damaged plasticity model (CDP) can be used. In ABAQUS, this model is offered as a way to assist in modeling the effects of loading on concrete, which is typically difficult due to its inelastic nature. The model is described in three ways in ABAQUS; the plasticity, the compressive behavior, and the tensile behavior. The data inputted for this model initially can be found in Appendix A. Additionally, data for compressive and tensile damages can be integrated into the model as well. Data for damage parameters used initially can be found in Appendix B. This data and more discussions about the concrete plasticity model will be covered in Chapter 5.

Lastly, the column shape was examined with the development of a circular column model. It was found that while the building of the model was simple, applying loads to the model presents a challenge due to the surface of the column not being naturally partitioned within ABAQUS. Thus, loads needed to be applied through the mesh surface of the column as opposed to the square column where the loads can be applied on the total surface. The solution to this issue will be addressed in Chapter 4, where the development of a workflow to effectively load any shape, including the circular column, is presented.

CHAPTER FOUR

4.1 - Development of a computational framework for uncoupled finite element analysis for UNDEX

This chapter presents the development of a framework for coupling externally created pressure profiles to ABAQUS. At the time of this thesis's writing, there are no plug-ins for the inclusion of pressures into ABAQUS from external programs automatically, thus several MATLAB algorithms are created to facilitate the transfer of pressure data to ABAQUS. The creation of a workflow from generation of externally-created pressure profiles to ABAQUS simulations allows for complex loading conditions to be achieved relatively easily and in turn makes parametric studies simpler to complete.

For the column analysis, ABAQUS splits the model into individual surfaces through the application of a mesh. The mesh's size is defined by the user. In this section, the mesh typically equals 50mm causing each element to have face sides equal to 50mm. Finer meshes will have more precision in the final simulation, however the simulation will require more time to analyze. An example of this mesh with individual surfaces can be seen in Figure 4.1.

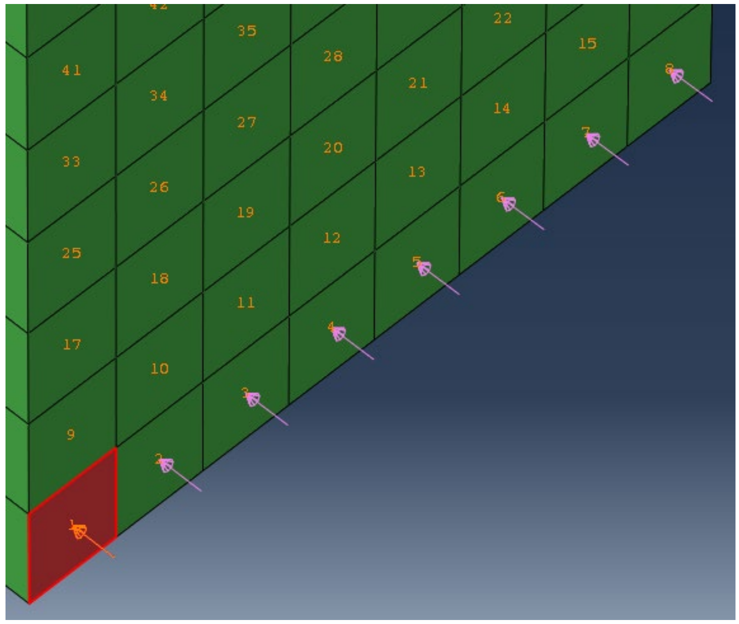

Figure 4.1. Example Surfaces seen on a Square Column.

As is the case of blast loading, the pressure loads placed on the column will not be uniform across the sides nor across the elements on one side. Thus, each individual element will have its own unique load and amplitude definition during the UNDEX event. The definition has three parts; the surface definition, the amplitude definition, and the load definition. The surface definition is based on the element number and is found through examining the column model mesh. This specifies the location of the particular element as well as what face of the element is experiencing the load. The amplitudes of the blast loadings are determined from Finite Element subsurface FLOW system (FEFLOW), a computational fluid dynamics code that is used on a variety of applications involving the analysis of protective structures. FEFLOW solves the compressible and incompressible Navier-Stokes equations for fluid flow, allows for diluted phases either as particles or continua, and has a large number of Equations of State (EOS), turbulence models, chemistry modules, and links to computational structural dynamics [30]. The FEFLOW pressures are then processed through a series of algorithms. These describe the multiplier that is applied to the load as well as the time that that multiplier is active for. For instance, an amplitude definition can describe a triangular decay by noting a multiplier of 1 at the beginning of the load case and a multiplier of 0 at the end. The load definition ties the other two definitions together as well as defines the magnitude of the amplitudes provided. The load and amplitude thus define the entire load that is applied. With this method, each element face can have a uniquely defined load.

4.2 - Development of MATLAB Code for integrating FEFLO loads into ABAQUS

4.2.1 - Circular Midpoint Generator

As noted previously, with finer mesh sizes comes an exponential increase in elements across the FEA model. Creating load, amplitude, and surface definitions for each of those elements manually would require a significant amount of time and effort. Additionally, in order to create these definitions, the midpoints of each outwardly-facing element are also required in order for FEFLOW to accurately develop loading conditions for ABAQUS. For the case of the square column, this is relatively simple to execute without the use of a program because the surface and midpoint numbers are easier to calculate and manipulate. However, due to the nature of the circular columns' elements and the nature of their surface numbers, the same process can take much more time. To remedy this issue, a series of MATLAB scripts were created for efficiency and for effectively developing midpoint definitions.

4.2.1.1 - Code Architecture

The code architecture for the midpoint generators revolves around a data sheet and several data points being fed into the program that then develops a full data sheet detailing the midpoints and surface definitions of every external element in the column. The data sheet fed into the program details the element numbers and their associated surface numbers of the first row of the circular column in examination. When the program is run, mesh size, column radius, and column height is inputted. Additionally, the increment at which the element number increases per row is also recorded. This is a static number throughout each element in a row and is used to help iterate through element numbers during the creation of the output spreadsheet. This phenomenon can be seen in Figure 4.2.

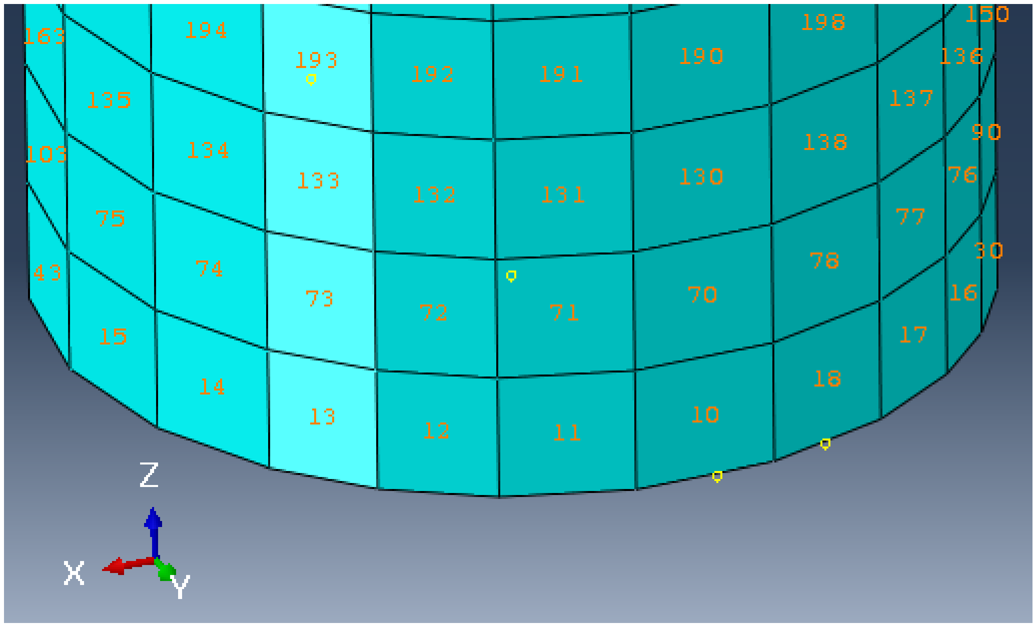

Figure 4.2. Illustration of Increasing Element Numbers per Row. Notice that the Element number increases by 60 per row in this example.

With the sixdata points of the element numbers, surface numbers, mesh size, column radius, clumn height, and element number increment, the column midpoints can be found.The MATLAB code takes the inputs and calculates each element's midpoint. This code relies on the caveat that the first element has its midpoint at x equals 0 and y equals the midpoint and moving clockwise. This is due to the fact that the element numbers in ABAQUS do not follow a specific pattern layer by layer, thus it is not possible to track whether the elements are in a clockwise or counterclockwise position or if the first element is truly at the top part of the column cross-section (0,radius).

Once the basic midpoint data is created, the MATLAB code then separates the data given the surface number, which is needed to assist the ABAQUS definition creator that is separated by surface number. The output of the code results in the full list of external elements' midpoints organized via surface number. The full code for this algorithm can be found in Appendix C. This data is then used to develop the FEFLO pressures that are used as inputs for the ABAQUS Definition Creator Code.

4.2.2 - Full ABAQUS Definition Creator

4.2.2.1 - Code Architecture

Once the various definitions are developed by the MATLAB scripts, they are placed into the existing model's input file. A noteworthy issue with the element surface definitions is the surface number notation. For C3D8R elements (8-node linear brick elements used for both the square and circular models) ABAQUS numbers its surfaces 1-6, and without that number the surface definition is invalid. Typically, only 4 of the 6 possible numbers are used for these loading cases presumably since the top and bottom surfaces hold the other 2 numbers. Thus, 4 different definition 'molds' need to be made for the variation in surface number. For the square column, each side of the square has a surface number associated with it. This causes every external face of each element on one side of the square to share the same surface number. For the circular column, each vertical stripe of the column has a surface number with no unifying side or direction to pinpoint the surface number. This is done by manually placing surface definitions on each element in one row of the circular column and examining the input file to determine the surface number. This is also done for the square column, however only 4 definitions are needed since there are 4 sides. Given that there are 4 surface numbers to consider, 4 different versions of the code were made to accommodate these surface numbers. Consider the following surface definition:

```
*Elset, elset="_Element 1 X Side_S2", internal, instance=PART-1-1
 1,
*Surface, type=ELEMENT, name="Element 1 X Side"
"_Element 1 X Side_S2", S2
```

Each definition is described by 4 lines. The first line describes the object being defined, additional parameters, and the instance the element is in. In this example, an object named “Element X Side” is being described. The ‘_S2’ at the end of the element name is added by ABAQUS and describes the surface number of the element face. The ‘internal’ moniker indicates that the element is within an internally created set by the program and typically indicates that the program is describing the element as part of the instance it spawns from. This additionally indicates that the location of the element is already stored earlier in the .inp file. The last part of the first line describes the instance that the element is in. For this example, ‘Element 1 X Side’ is part of the instance ‘PART-1-1’. The second line of the definition describes the element number of the element described. For this example, this number is ‘1’. The third line describes the type of definition, type of object being analyzed, and the name of the object. The last line simply restates the element name as well as the surface number of the element surface being analyzed.

Having created a framework for what changes between elements' surface definitions, algorithms can be written to describe every element's surface definition. Given the strategy developed previously, element numbers can be linked to their corresponding surface numbers to create a full surface definition. In the case of the integrating FEFLO pressure data, this means that each set of pressure data can be separated by surface number leading to the creation of the four molds discussed earlier. Table 4.1 shows a sample set of data for the surface number 1 elements.

Table 4.1. Sample Amplitudes for Surface Number 1

Time (s)	Elements							
	4145	4146	4147	4148	4149	4150	4151	4152
0.00E+00	1.00E+06	1.00E+06	1.00E+06	1.00E+06	1.00E+06	1.00E+06	1.00E+06	1.00E+06
1.46E-04	1.01E+06	1.01E+06	1.01E+06	1.01E+06	1.01E+06	1.01E+06	1.01E+06	1.01E+06
1.50E-04	1.01E+06	1.01E+06	1.01E+06	1.01E+06	1.02E+06	1.01E+06	1.01E+06	1.01E+06
1.54E-04	1.01E+06	1.01E+06	1.01E+06	1.02E+06	1.03E+06	1.02E+06	1.01E+06	1.01E+06
1.58E-04	1.01E+06	1.01E+06	1.02E+06	1.03E+06	1.04E+06	1.03E+06	1.02E+06	1.01E+06
1.62E-04	1.01E+06	1.02E+06	1.03E+06	1.04E+06	1.05E+06	1.04E+06	1.03E+06	1.02E+06
1.66E-04	1.02E+06	1.03E+06	1.04E+06	1.05E+06	1.06E+06	1.05E+06	1.04E+06	1.03E+06

For each element listed, the pressure applied at the time in the first column is listed. The pressure is in units of centimeter-gram-seconds and is converted into pascals inside ABAQUS. To integrate the data into MATLAB, a series of for-loops are used to tabulate the data into matrices that can then be manipulated to create definitions that ABAQUS can interpret. This process is the basis of the full definition creator. Figure 4.3 shows the code for the first two lines of the surface definition. In this snippet, the code creates a surface definition based solely off the element numbers with the corresponding surface number given from the midpoint generation done earlier. The amplitude and load definition creators follow a similar process of gleaning data from the input table and creating definitions based on it.

```
%% Surface Generation

for elenum = 2:datasize(1,2)
    %Many of the routines in this script refer to 'data(1,elenum)'. This
    %term takes the first row of the table (the element numbers) and runs
    %them through a for-loop that create a display statement to follow the
    %template below.

    formatSpec = '*Elset, elset="_Element %d X Side_S1", internal, instance=Part-1-1\r\n';
    fprintf(fileID,formatSpec,data(1,elenum));
    fprintf(fileID,'%d,\r\n',data(1,elenum));
end
%*Elset, elset="_Element 1 X Side_S2", internal, instance=PART-1-1
%  1,
```

Figure 4.3. MATLAB code for the first half of the Surface Definition Creator

Figure 4.4 shows a sample of the surface definitions generated by the algorithm. Separate algorithms were made to accommodate the circular columns in similar fashion with some complications.

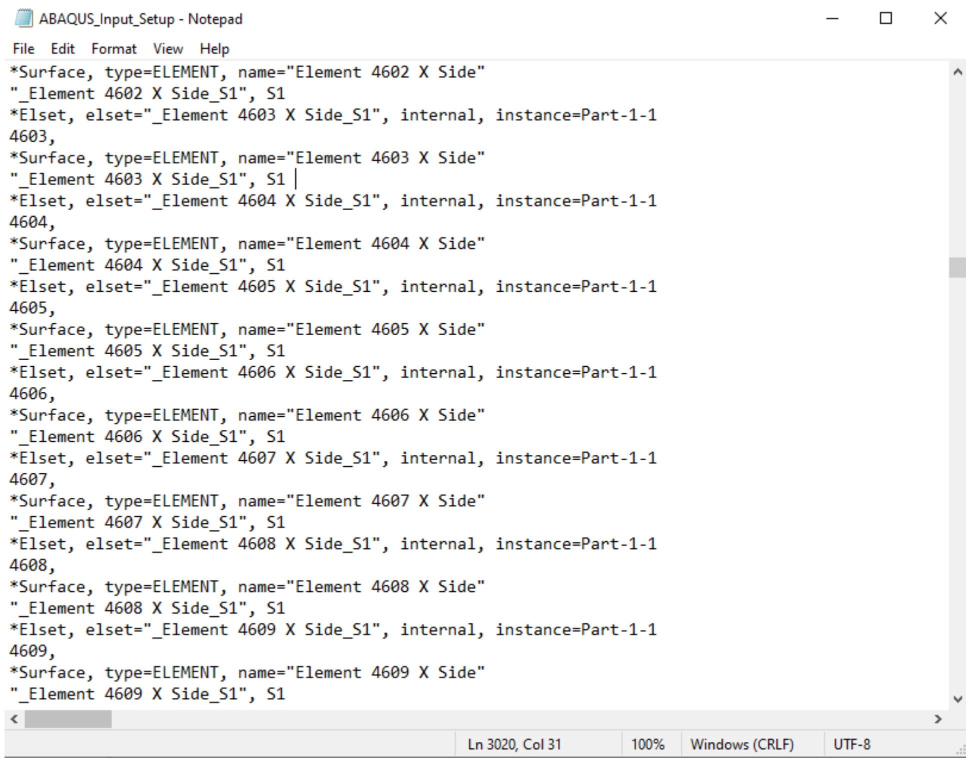

ABAQUS_Input_Setup - Notepad

File Edit Format View Help

```
*Surface, type=ELEMENT, name="Element 4602 X Side"
"_Element 4602 X Side_S1", S1
*Elset, elset="_Element 4603 X Side_S1", internal, instance=Part-1-1
4603,
*Surface, type=ELEMENT, name="Element 4603 X Side"
"_Element 4603 X Side_S1", S1
*Elset, elset="_Element 4604 X Side_S1", internal, instance=Part-1-1
4604,
*Surface, type=ELEMENT, name="Element 4604 X Side"
"_Element 4604 X Side_S1", S1
*Elset, elset="_Element 4605 X Side_S1", internal, instance=Part-1-1
4605,
*Surface, type=ELEMENT, name="Element 4605 X Side"
"_Element 4605 X Side_S1", S1
*Elset, elset="_Element 4606 X Side_S1", internal, instance=Part-1-1
4606,
*Surface, type=ELEMENT, name="Element 4606 X Side"
"_Element 4606 X Side_S1", S1
*Elset, elset="_Element 4607 X Side_S1", internal, instance=Part-1-1
4607,
*Surface, type=ELEMENT, name="Element 4607 X Side"
"_Element 4607 X Side_S1", S1
*Elset, elset="_Element 4608 X Side_S1", internal, instance=Part-1-1
4608,
*Surface, type=ELEMENT, name="Element 4608 X Side"
"_Element 4608 X Side_S1", S1
*Elset, elset="_Element 4609 X Side_S1", internal, instance=Part-1-1
4609,
*Surface, type=ELEMENT, name="Element 4609 X Side"
"_Element 4609 X Side_S1", S1
```

Ln 3020, Col 31 | 100% | Windows (CRLF) | UTF-8

Figure 4.4. Example of Surface Definitions for Square Column

For the amplitude, the data required to create the definition comes from FEFLO. Each element surface will have a corresponding set of data associated with it; the time during which the pressure is being applied and the pressure magnitude. Consider the following ABAQUS amplitude definition;

*Amplitude, name=Amplitude3274, time=TOTAL TIME

0.00000000, 1000000.00,

0.00050470, 1020000.00,

0.00050930, 1020000.00

The amplitude definition is at most 2 lines. The first line indicates a new amplitude definition with its name and the timeframe that it is operating in. For this set of studies, ‘TOTAL TIME’ refers to the simulation’s total runtime from the beginning of the simulation to its end. This could change based on the timesteps analyzed. The following lines describe the time and pressure magnitude. For the example given above, the first instance of loading occurs at 0s at a magnitude of 1000000 units (it is important to note that ABAQUS does not have built in units for anything that is not time). The second instance of loading occurs at 0.00050470s at a magnitude of 1020000 units and so on. Given this model and having both the element number that the loading is applied to and the loading condition, creating amplitude definitions for each element can be automated. The amplitude naming convention is simply “Amplitude” followed by the element number to ease analysis of individual elements and to facilitate creation of the final definition: load.

The load definition ties together the surface and amplitude definitions as well as adds key details to fully round out the loading conditions. Consider the following load definition:

```
** Name: SURFFORCE-4306   Type: Pressure
*Dsload, amplitude=Amplitude4306
Part-1-1."Element 4306 Surface", P, 1e-07
```

The load definition is made up of two lines. The first line shown is predicated by ‘**’. Similar to MATLAB’s ‘%’ or Java’s ‘/*’ & ‘*/’, this notation dictates a comment within the code. This line additionally lists the name of the force (generated by the algorithm) and the type of loading. This has the benefit of clarity as the name of the load correlates with the element number similar to the surface and amplitude definitions. The shared trait between the three verifies that the correct loading condition has been established. The second line begins with "*Dsload", signifying that the load is distributed with the amplitude that follows. As seen in the example, the amplitude "Amplitude4306" is used which matches the load name. The third line in order indicates the instance, the surface, the load type, and the loading magnifier. It is known from previous definitions that element 4306 is a part of instance Part 1-1. The "P" denotes a pressure loading as opposed to other types of loading such as a point load or a line load. Lastly, the number following the load type denotes the magnitude that is multiplied to the amplitude. The load definition ties together the previously made definitions and adds key information to allow for a full loading condition on one element. With this set of algorithms, a full loading condition can be created for a column and imported into ABAQUS. Figure 4.5 demonstrates a fully loaded circular column created with this method. The full code for the surface, amplitude, and load definition creators for one surface number can be found in Appendix C. While there are other algorithms, the key difference is only in the surface number designation and is not varied from the original 'mold' algorithm.

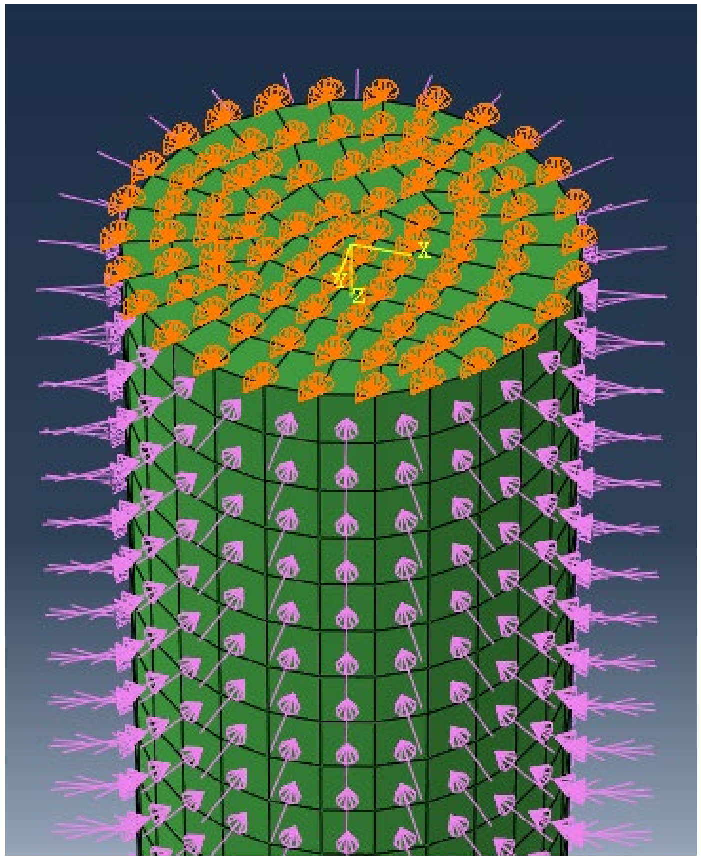

Figure 4.5. Fully Loaded Circular Column developed through MATLAB Algorithms

In summary, the process for analyzing an UNDEX scenario in ABAQUS is as follows; the basic column model is made including reinforcement details and material properties. The file is analyzed to find the surface numbers of each of the elements, and a file detailing the midpoints of each of the elements is created. An UNDEX event is modeled by others, such as FEFLO from George Mason University's Center for Fluid Dynamics, and the amplitude-time data for each element is provided. This file is then processed through the MATLAB scripts developed by this research which generates surface, amplitude, and load definitions that can be read in ABAQUS's input file system. The input file is imported into ABAQUS, generating a final model which includes the

FEFLO pressure data. This model is then run through a simulation, resulting in a series of output data such as displacement profiles, stress-strain graphs, and other information. Figure 4.6 shows the workflow.

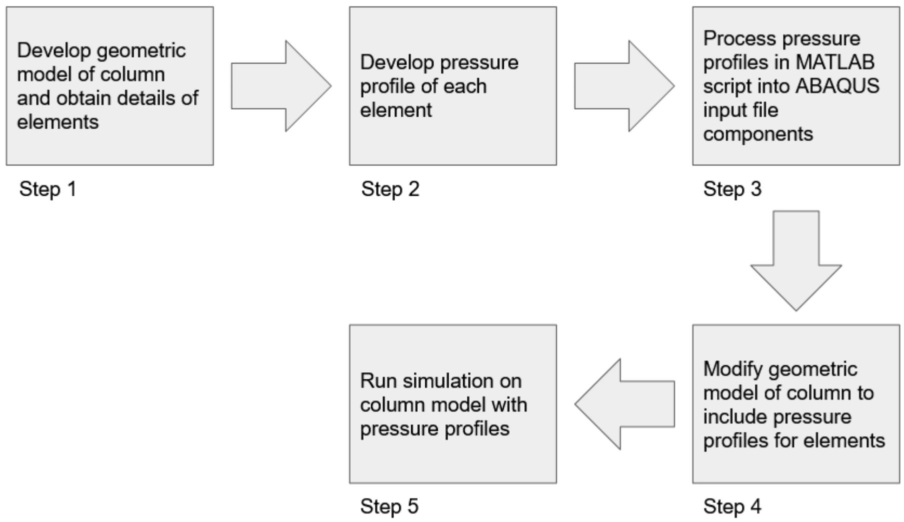

Figure 4.6. Workflow of analyzing RC column UNDEX events (uncoupled analysis)

In conclusion, this chapter presents the development of algorithms for uncoupled analysis of RC columns subjected to UNDEX in ABAQUS where pressures from external computational fluid dynamics codes are provided. The circular midpoint generator code is used to develop midpoints for assisting in the creation of the FEFLO pressures. The FEFLO pressures are then processed through the ABAQUS definition creator algorithms to generate pressure profiles readable by ABAQUS. With this workflow in mind, variations on the UNDEX scenario including effects on both the explosive and the column configuration can be achieved. Thus, parametric studies can be completed with relative ease.

CHAPTER FIVE

5.1: Concrete Damage Plasticity (CDP) Model

ABAQUS uses the concrete damage plasticity (CDP) model. This model is largely based on the relationships between stress and strain, however the exact equations used to model these relationships vary. This is due to the complexity of the material; concrete is not a completely elastic material nor is it completely ubiquitous between different performance denominations. Thus, selection of the proper model is critical. The main feature of the concrete damage plasticity model is the use of scalar damage variables measuring the damage of the material from 0 to 1 (or undamaged to destroyed) represented by d_c and d_t. Urgessa [31,32] examined multiple proposed models for the stress-strain relationship of concrete. Three separate models were examined by Urgessa. Out of the three, the model proposed by Collins et al. [33] was chosen to represent concrete in this thesis. This model makes use of the relationship between compressive stress and maximum stress with regards to strain represented in Equation 5.1, Equation 5.2, Equation 5.3, Equation 5.4, and Equation 5.5.

$$\frac{fc}{f'c} = \frac{\varepsilon_c}{\varepsilon'_c}\frac{n}{n-1+(\varepsilon_c/\varepsilon'_c)^{nk}} \tag{5.1}$$

Where $n = 0.8 + \frac{f'_c}{17}$ in MPa units (5.2)

And $k = 1$ for the ascending part of the curve and $k = 0.67 + \frac{f'_c}{62}$ for the descending part in MPa (5.3)

$$\varepsilon'_c = \frac{f'_c}{E_c}\frac{n}{n-1} \tag{5.4}$$

$$E_c = 3320\sqrt{f'_c} + 6900 \text{ in MPa} \tag{5.5}$$

Where f_c is the compressive strength, f'_c is the characteristic compressive strength, ε_c is strain, ε'_c is the strain at maximum stress, and E_c is the initial modulus of elasticity. This allows for high-performance concrete (HPC) to be represented more accurately by accounting for its sharper drop in the stress-strain strain curve compared to conventional concrete. Additionally, the compression damage model used in ABAQUS makes use of a modified equation from Popovics [34] shown in Equation 5.6 for the damage variable. Equations 5.7, 5.8, 5.9, and 5.10 support the damage variable calculation.

$$d_c = 1 - \frac{\sigma_c {E_c}^{-1}}{{\varepsilon_c}^{pl}(1/b_c - 1) + \sigma_c {E_c}^{-1}} \tag{5.6}$$

$${\varepsilon_c}^{pl} = b_c {\varepsilon_c}^{in} \tag{5.7}$$

$${\varepsilon_c}^{in} = \varepsilon_c - \sigma_c {E_c}^{-1} \tag{5.8}$$

$$\sigma_c = nE_s\varepsilon_c/[n - 1 + (\varepsilon_c/\varepsilon'_c)^{nk}] \tag{5.9}$$

$$E_c/E_S = n/(n - 1) \tag{5.10}$$

Where d_c is the compressive damage coefficient, σ_c is compressive stress, ${\varepsilon_c}^{pl}$ is plastic strain, ${\varepsilon_c}^{in}$ is inelastic strain, b_c is a minimizing coefficient determined via experiments performed by Popovics [34], and E_S is the secant modulus of elasticity.

These models create a stress-strain curve that is able to model the compressive behavior of the concrete, thus allowing for damage to be examined.

The tensile behavior of the concrete is a modified version of a tensile model developed by Belarbi and HSU [35] represented by Equations 5.11, 5.12, 5.13, 5.14, and 5.15.

$$\sigma_t = f'_t(\frac{\varepsilon_{ct}}{\varepsilon_t})^{0.4} \tag{5.11}$$

$$d_t = 1 - \frac{\sigma_t {E_c}^{-1}}{{\varepsilon_t}^{pl}(1/b_t - 1) + \sigma_t {E_c}^{-1}} \tag{5.12}$$

$$f'_t = 0.63\sqrt{f'_c} \tag{5.13}$$

$$\varepsilon_c{}^{pl} = b_t \varepsilon_t{}^{in} \tag{5.14}$$

$$\varepsilon_t{}^{in} = \varepsilon_t - \sigma_t E_c{}^{-1} \tag{5.15}$$

Where σ_t is tensile stress, f'_t is the characteristic tensile strength, ε_{ct} is initial strain, ε_t is strain, d_t is the tensile damage coefficient, E_c is modulus of elasticity, $\varepsilon_t{}^{pl}$ is plastic strain, and $\varepsilon_t{}^{in}$ is inelastic strain.

This is not the entirety of the concrete damage plasticity model within ABAQUS. For the plasticity portion of the model, ABAQUS makes use of the research by Lubliner [36] and Lee & Fenves [37]. Lee and Fenves developed a model through examining a cyclically loaded concrete sample. Their research consists of comparing the results of previous experiments conducted by Karsan & Jirsa [38] and Gopalaratnam & Shah [39] with an independently created set of relationships. Their model focused on continuum damage mechanics and the use of fracture-energy-based multiple-hardening variables for representing compressive and tensile damage separately. The use of an additional variable accounted for the elastic response of the sample for evaluating erosion and stress on the concrete. Lubliner also developed a plasticity-damage model through analyzing a variety of prior experiments and focusing on the multi-faceted problems plasticity analysis can tackle.

For the purposes of dynamic response verification of a reinforced concrete column subjected to UNDEX in section 5.2 of this thesis, the CDP parameters shown in Appendix A were selected as a baseline. The model makes use of five separate variables; the dilation angle, the eccentricity, the ratio of the strength of the concrete in the biaxial state to the uniaxial state, stress intensity factor, and the viscosity parameter. These variables are derived from the work of Lubliner [36] and Lee & Fenves [37]. Understanding how changes in these variables dictate the viability of ABAQUS to predict structural response for UNDEX is important, thus sensitivity studies were conducted and discussed in section 5.3.

5.2: Dynamic Response Verification

Using the baseline CDP model, the response of RC columns for UNDEX can be studied within ABAQUS. The CDP model is more critical for dynamic loading scenarios compared to the static analysis presented in Chapter 3. Appendix A includes the CDP model parameters used for dynamic response verification.

There are empirical equations available for benchmarking free-field peak pressure and impulse generated due to an underwater explosion. Before conducting a full FEFLO validation, peak pressure and impulse values reported in experimental tests are compared with empirical equations reported in Cole [1], Swisdak [40], and Kevin and Hempen [41]. The empirical equations typically are derived from an exponential decay pressure-time function (P-t) as shown in Eqn. 5.16.

$$P = P_m e^{-t/\theta} \tag{5.16}$$

where P_m is the initial peak pressure and θ is the time it takes for the pressure to decay to a value of 1/e.

Based on 122 records using Pentolite charges, Cole [1] presented one of the earliest empirical equations available for predicting P_m and the respective impulse (I) was found by integrating the exponential decay function. A time interval of (6.7θ) is typically used for impulse calculations. Recognizing TNT is the standard high explosive and the need to accommodate other types of charges, Cole [1] presented power laws shown in Eqn. 5.17 where W is the weight of the explosive, R is the stand-off distance, k and α are corrective coefficients, and Z is the scaled distance.

$$P_m = k(\frac{W^{1/3}}{R})^{\alpha} = k(\frac{1}{Z})^{\alpha} \quad (5.17)$$

Eqns. 5.18, 5.19 and 5.20 apply for pressure, time constant and impulse in the US customary units when the explosive is TNT.

$$P_m = 2.16 * 10^4(\frac{W^{1/3}}{R})^{1.13}, \text{ where } P_m \text{ is in psi, } W \text{ is in lb, and } R \text{ is in ft} \quad (5.18)$$

$$\theta = 6 * 10^{-2} W^{1/3}(\frac{W^{1/3}}{R})^{-0.18}, \text{ where } \theta \text{ is in seconds} \quad (5.19)$$

$$I = 1.46W^{1/3}(\frac{W^{1/3}}{R})^{0.89}, \text{ where I is in psi*s} \quad (5.20)$$

These equations are used to simulate a blast load on a sample RC column. These studies are meant to provide an estimation of a loading scenario. The loading applied will consist of a UDL with maximum pressures developed via Cole's equations [1] adjusted by proper reflection coefficients. These pressures are based on explosives of varying quantities with a standoff distance of 1m. Zhuang [25] ran several experiments making use of a submerged RC column where pressures and displacements of the column were recorded for varying blast scenarios. Table 5.1 shows the maximum pressures obtained from the experiments conducted by Zhuang [25] and results obtained from Cole's equations [1], Figure 5.1 and Figure 5.2 show these pressure differences compared to scaled distance (Z) and explosive quantity. A reflection coefficient of 2 was applied to Cole's pressures because the empirical equations are developed to capture free-field pressure without an obstacle, such as the RC column here. These comparisons show that Cole's equations are conservative however they are still within acceptable range of the experimental values. Additionally, the variability of the empirical pressures increases at lower-weight explosives.

Table 5.1: Comparison of Zhuang's Pressures to Pressures from Empirical Equations

Explosive Quantity (kg)	Scaled Distance ($m/kg^{1/3}$)	Experimental Max Pressures (MPa)	Empirical Max Pressures (MPa)
0.05	2.71	28.43	34.00
0.20	1.71	54.16	57.16
0.40	1.36	77.92	74.22

0.80	1.08	102.64	96.33

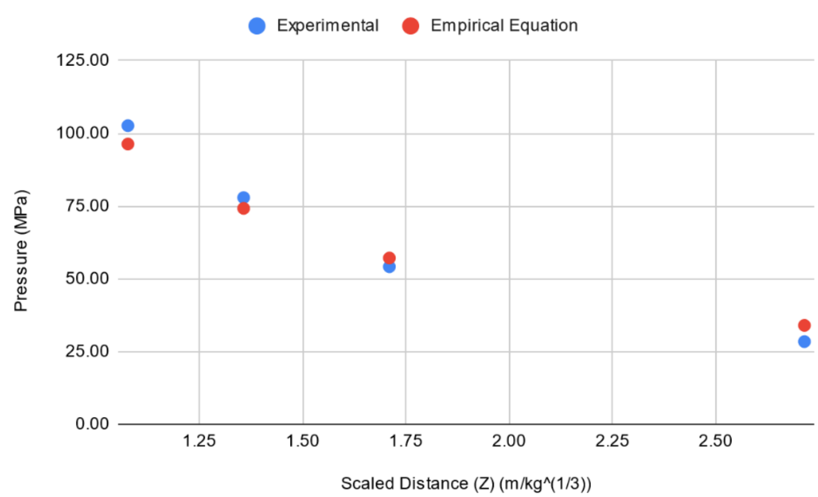

Figure 5.1: Pressure Value Comparison between Experimental and Empirical Equations Relative to Scaled Distance

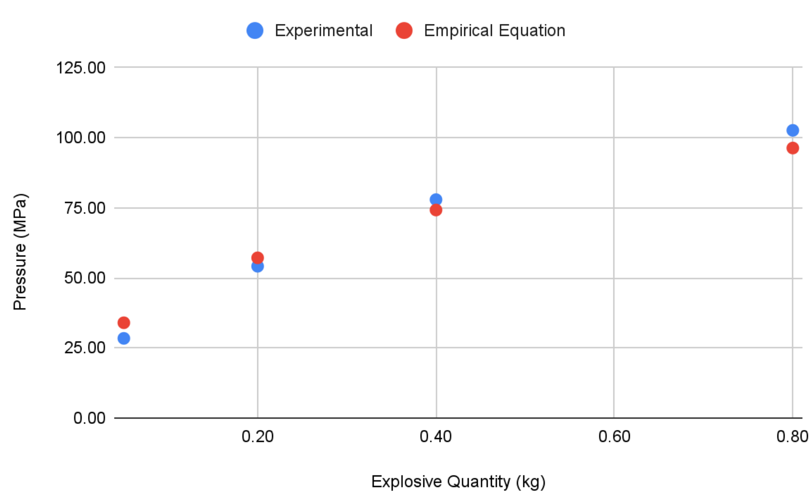

Figure 5.2: Pressure Value Comparison between Experimental and Empirical Equations Relative to Explosive Quantity

With the pressures verified, the question of how much time the simulated blast lasts becomes relevant. Due to the nature of blast, the same amount of time used to reach ϴ cannot be used for the UDL as the impulses would not match. Additionally, the blast duration used in Zhuang's experiments were not described sufficiently in their report. Thus, trials were conducted to examine how long the UDL should last for. A RC column model was created with a cross-section dimension of 100mm by 100mm by 2500mm, reinforced with four longitudinal reinforcement rebars with a cross-sectional area of 56.55mm. This column model is based on Zhuang's column with a similar compressive strength of 52MPa and reinforcement ratio. The UDL trials were compared to the displacements found by Zhuang at the midpoint of the column. The UDL is applied with triangular decay such that the pressure linearly decreases to 0 at the end of the loading time. Figure 5.3 shows the values obtained from the trials compared to Zhuang's data. It is shown that for the UDL blast scenario, a blast time of 0.8ms on average is the closest approximation to a realistic blasting scenario when comparing the maximum displacement of the column at its midpoint. These values, while conservative, are due to the consideration of using a UDL as opposed to a more complex loading scenario that is more accurate to a real blast scenario. This demonstrates the ability of the empirical equations to give a rough estimate of a blasting scenario and demonstrates the validity of the CDP model for dynamic loading. With this in mind, sensitivity studies can now be conducted to analyze how changes on the CDP input variables affects the dynamic response.

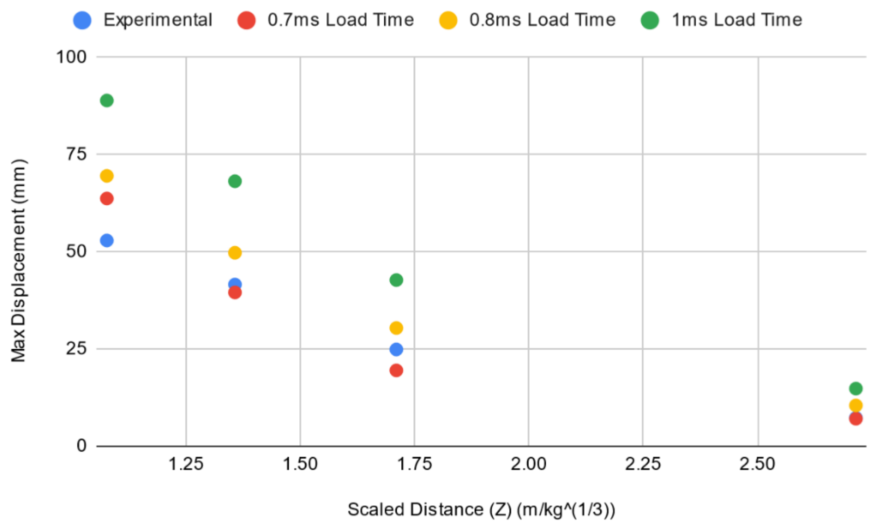

Figure 5.3: Displacement Comparisons of Experimental Values and Varying Blast Load Times

5.3: Sensitivity Studies

This section presents a series of sensitivity studies where the values within the CDP material model parameters are altered to analyze their effects on the maximum displacement of the column when subjected to an UNDEX load. Additionally, the mesh size and Poisson's ratio are also examined. The load used is the same load tested for the 0.4kg explosive quantity triangularly decaying to 0.8ms. Each parameter was tested separately with the other parameters holding the same values as those shown in Appendix A.

At the outset, it is critical to determine if the mesh size alters the data retrieved from the UNDEX simulation. The expectation is that for the same node in the same position between mesh changes, the data should remain the same as the column is under the same load. Thus, the only change is a higher amount of data for the column as a whole due to the generation of more nodal points. As seen in Figure 5.4, the mesh size with the range of 25mm (~1 inch) did not affect the displacement data significantly. Additionally, adaptive mesh sizes are often used to solve computational errors within ABAQUS, so understanding that the response remains more or less unchanged increases confidence in the analysis.

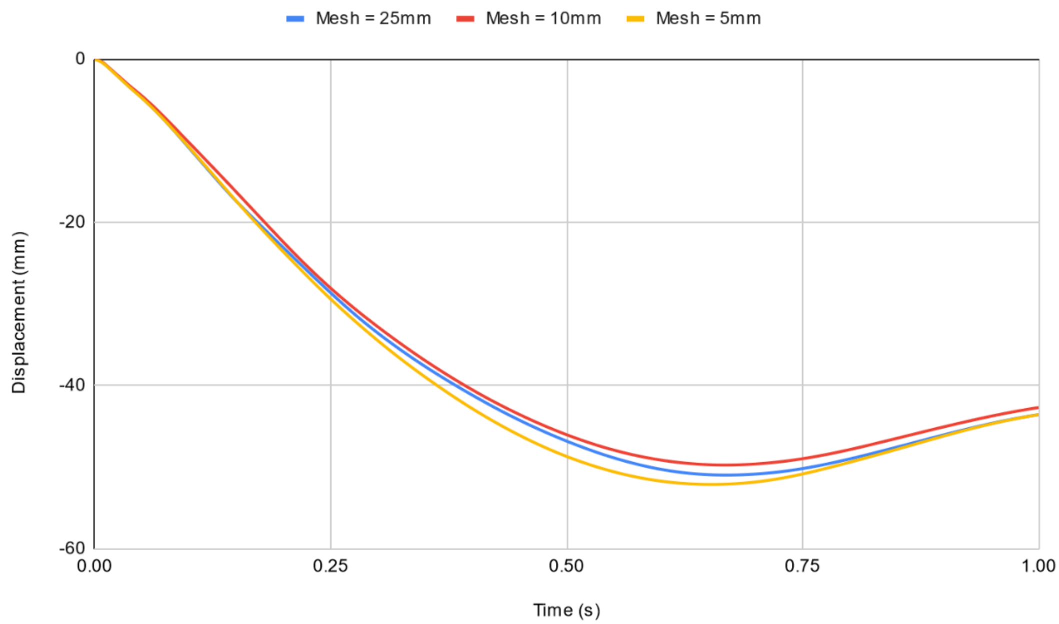

Figure 5.4: Examination of Change on Mesh Size on Front Face Central Node Displacement

Examination of Poisson's ratio, while not part of the CDP input parameters, is critical for material models. In the case of concrete, the ratio falls between 0.15 to 0.25 which may affect the response of the material depending on the value. As seen in Figure 5.5, the maximum displacement decreases with increased Poisson's ratio. This result is acceptable as higher values of Poisson's ratios indicate stiffer response.

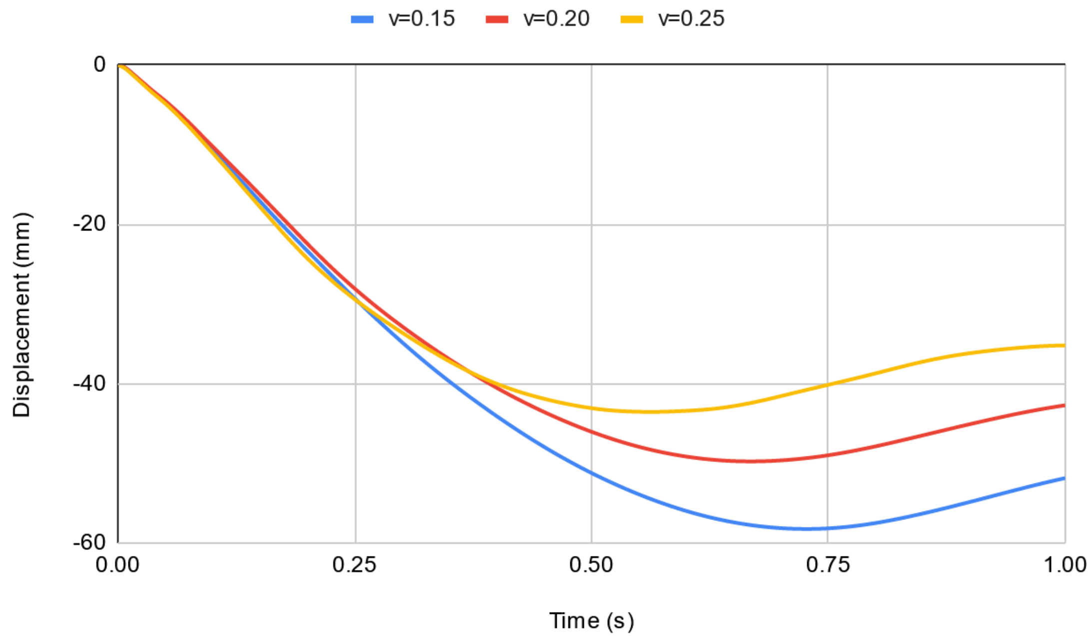

Figure 5.5: Examination of the Effect of Poisson's Ratio on Front Face Central Node Displacement

The dilation angle of the CDP model is typically recommended to fall between 30°-40°, however dilation angles as low as 5° have been reported in literature [42] Sensitivity studies were conducted on the range of dilation angle values from 10°-40°. Figure 5.6 displays the displacement of the central node with different dilation angle values. It is shown that with an increasing dilation angle, the maximum displacement of the center of the column decreases.

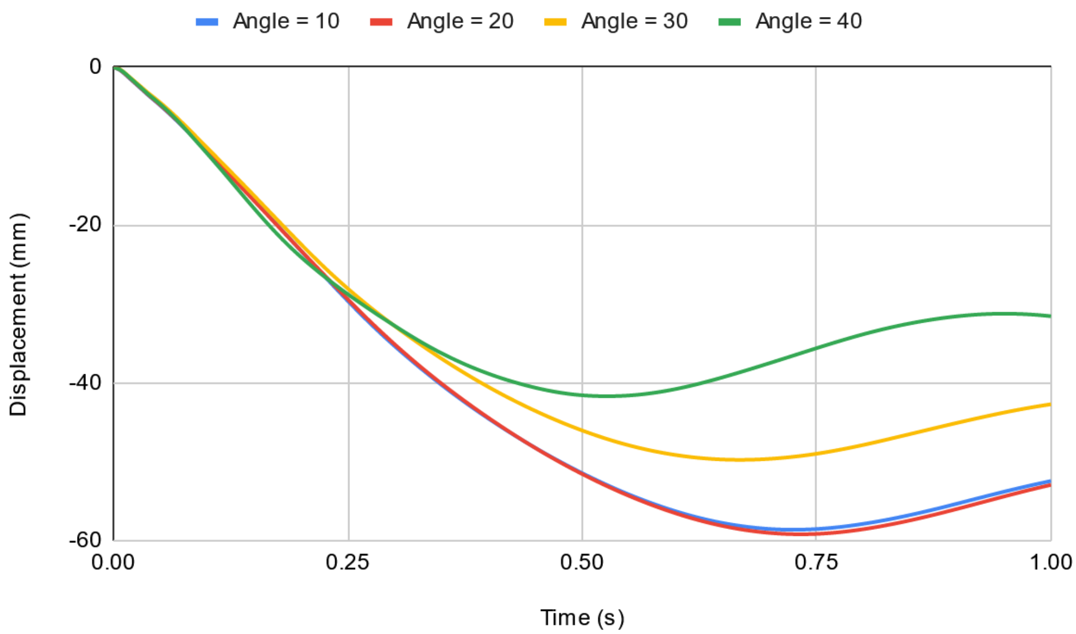

Figure 5.6: Examination of the Effect of Dilation Angle on Front Face Central Node Displacement

The effect of the ratio of initial biaxial compressive yield stress to initial uniaxial compressive yield stress on center node displacement is shown in Figure 5.7. ABAQUS uses a default value of 1.16. It is shown that with an increase in the ratio, the central node displacement increases. Given this result, it is implied that the biaxial compressive yield stress has a larger effect on the displacement.

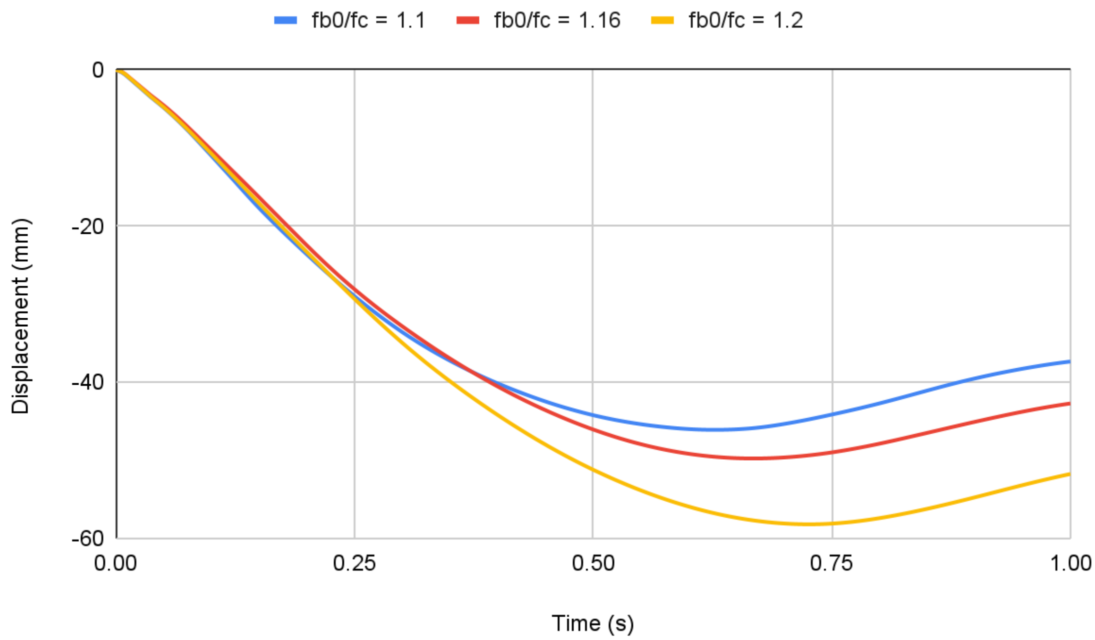

Figure 5.7: Examination of the Effect of Ratio of Initial Biaxial Compressive Yield Stress and Initial Uniaxial Compressive Yield Stress on Front Face Central Node Displacement

The effects of the ratio of the second invariant of the stress deviator on the tensile meridian to the compressive meridian (K) are shown in Figure 5.8. For this study, a range of 0-1 was examined. As shown, the displacements as the K changes are close, however no conclusions can be confidently drawn from this result. It is notable that the minimum recommended value of K is 0.5 [36], however ABAQUS did not fail at K = 0. This implies that ignoring K is a viable option for simulation, however further research into the effects of altering K is recommended for future study.

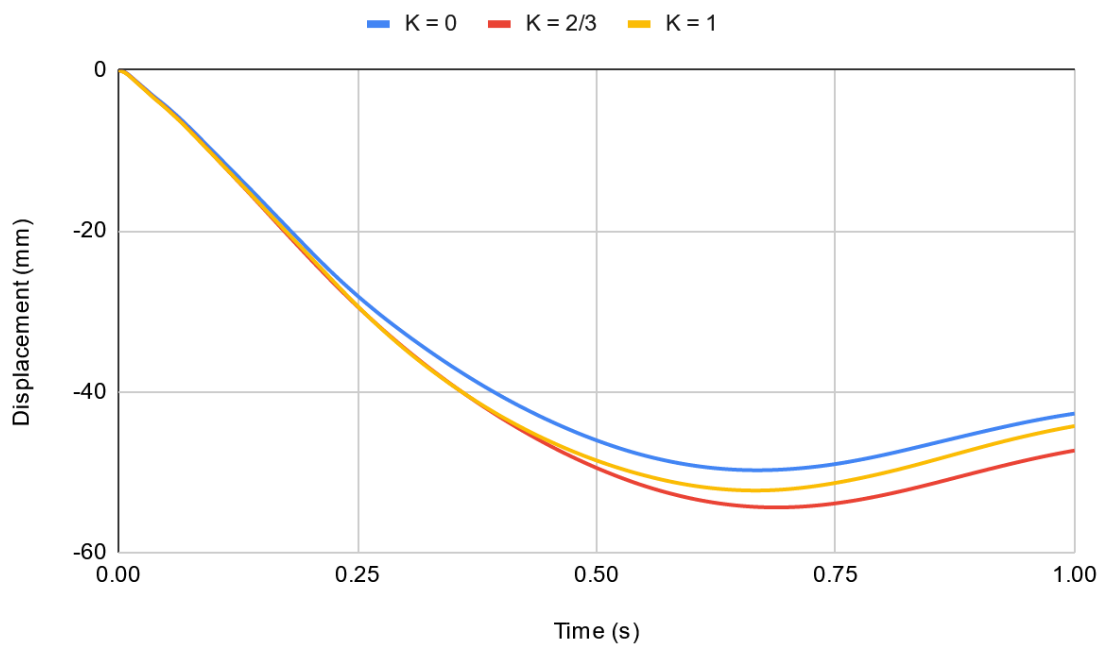

Figure 5.8: Examination of the Effect of K on Front Face Central Node Displacement

Within CDP, the viscosity parameter in ABAQUS is used as a method to force the solution to converge. Altering the parameter can help create a set of results, however verification of the results is necessary to qualify it as a way to help solve problematic simulations. Figure 5.9 shows the effects of varying the viscosity parameter within the range of 0-0.1. As shown, altering the viscosity parameter has little effect on the displacement-time history of the central node. Notably, the results for viscosity = 0, viscosity = 0.05, and viscosity = 0.1 are the same.

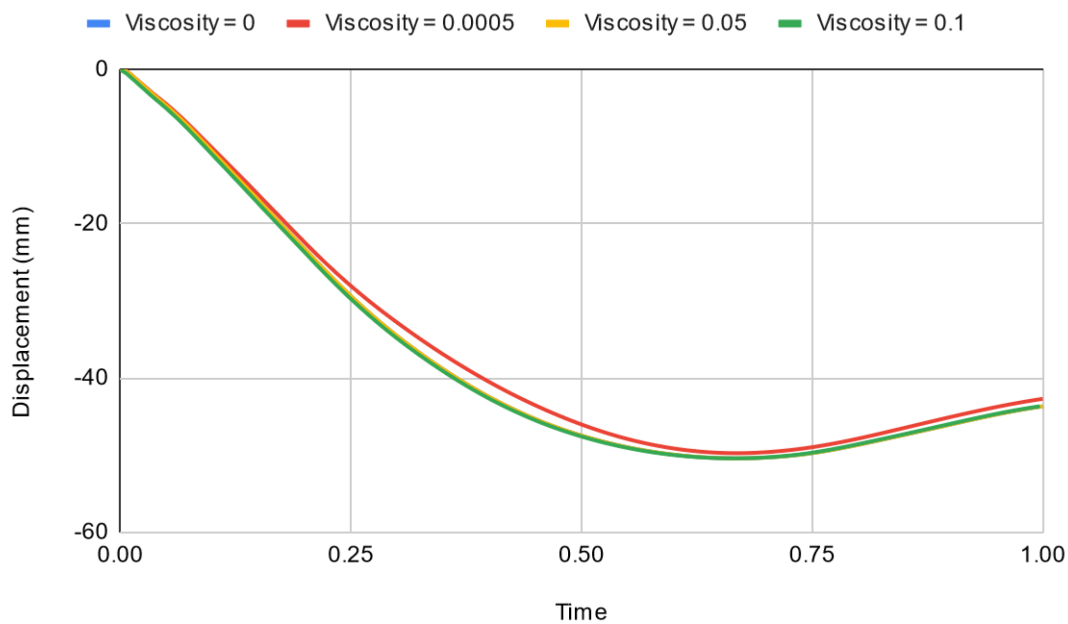

Figure 5.9: Examination of the Effect of Viscosity on Front Face Central Node Displacement

CHAPTER SIX

6.1: Conclusions

In this thesis, a series of studies were conducted on the topic of the effects of UNDEX on RC structures. First, a thorough literature review examining the methods and experiments performed with UNDEX was presented. It was found that much of the literature focused on ship effects and less on the effect of concrete structures such as dams and piers. Additionally, research into computational methods and the physical phenomena of UNDEX was also explored. A computational framework was developed to help facilitate the integration of CFD loads into ABAQUS. This framework consists of a series of MATLAB programs designed to create loading definitions from spreadsheets into a format readable by ABAQUS. This eases the application of complex loading scenarios in ABAQUS and thus allows for complex loading scenarios like UNDEX to be analyzed efficiently. This shows that the usage of an uncoupled analysis method is effective when analyzing UNDEX. A dynamic response verification was also provided comparing pressure results from published experimental values with those obtained from empirical equations, and comparing measured displacements with ABAQUS outputs. The results showed that the empirical equations compared favorably with the physical results, increasing confidence in their usage for modeling UNDEX effects. This led to the creation of the fast-running model. Lastly, an examination of the CDP model was conducted including sensitivity studies of the input parameters. It was found that alteration of the CDP parameters had a wide range of effects and caution must be exercised when using these parameters in finite element analysis without actual material test data.

6.2: Limitations and Future Research

The limitations of the study stem from three main points. First, this thesis focused on the usage of computational programs for analysis, but the data used to verify the results is dependent on small-scale experiments conducted by others. Thus, limitations in experimental setup or the unreported experimental parameters, such as the time of duration of blast, may affect the results of the studies. Additionally, ABAQUS only has the CDP material model with no alternatives for comparison. However, other FEA programs, such as LS-DYNA have incorporated additional concrete models, such as the Karagozian and Case concrete model (KCC). Further studies into the comparison of those material models are recommended. Lastly, the integration of FEFLO loads using the computational framework detailed in this thesis is specific to ABAQUS. Further research into either porting over the current framework or creation of new frameworks for use in other FEA programs is recommended.

Future studies on the topic of simulating UNDEX effects on RC columns include improvements to the computational framework, usage of the framework in coupled analysis, and future sensitivity studies into the CDP material models (such as K and viscosity values). The computational framework currently relies on an already built column to develop its loading definitions, however ABAQUS tabulates the geometry details in the same file the loading definitions are placed when a new model is created. The use of programs to automatically create column geometries without usage of ABAQUS's graphic user interface would vastly decrease the time needed to create models for analysis. Additionally, use of the framework to model externally-generated FEFLO loads to analyze ABAQUS models would prove a worthwhile study. As noted in Chapter 5, the K value proved to be sensitive to maximum displacements and further examination is recommended. Similarly, the viscosity sensitivity study showed that the effects of increasing the parameter diminish after a threshold value and further study is needed to outline a recommendation for analysts. Lastly, examination into element deletion within the finite element simulations is recommended.

APPENDIX A - CONCRETE DAMAGED PLASTICITY MODEL & ELASTIC PROPERTIES FOR CONCRETE

Plasticity				
Dilation Angle	Eccentricity	fb0/fc0	K	Viscosity Parameter
30	0.1	1.16	0	0.0005
Compressive Behavior				
Yield Stress (Pa)	Inelastic Strain			
40000000	0			
Tensile Behavior				
Yield Stress (Pa)	Inelastic Strain			
5000000	0			

APPENDIX B - COMPRESSIVE AND TENSILE DAMAGE BEHAVIOR OF CONCRETE IN INITIAL TESTING

Compression				Tension			
Yield Stress (MPa)	Inelastic Strain	Damage Parameter	Inelastic Strain	Yield Stress (MPa)	Cracking strain	Damage Parameter	Cracking strain
15.6	0	0	0	4.542994607	0	0	0
21.50907111	2.58E-06	0.001108041	2.58E-06	3.07510429	0.000291062	0.724305698	0.000291062
30.39574961	1.44E-05	0.00437394	1.44E-05	2.533541651	0.000552088	0.858126181	0.000552088
38.53982911	5.04E-05	0.011946599	5.04E-05	2.224792951	0.000805565	0.909504857	0.000805565
45.27893524	0.000131852	0.026235745	0.000131852	2.017252094	0.00105576	0.935595792	0.00105576
52	0.000589779	0.094972067	0.000589779	1.864755894	0.001304171	0.951010404	0.001304171
46.15024824	0.001081636	0.178204537	0.001081636				

37.35290356	0.001669068	0.292499028	0.001669068				
28.33869721	0.002263531	0.424962427	0.002263531				
20.75766202	0.002811524	0.556181499	0.002811524				
15.01326994	0.003299965	0.670366929	0.003299965				
10.87187123	0.00373643	0.760754299	0.00373643				
7.941578215	0.004133625	0.828055775	0.004133625				
5.872176362	0.004502906	0.876464249	0.004502906				
4.400803819	0.004852797	0.910734437	0.004852797				
3.343097231	0.005189274	0.934902965	0.005189274				
2.573015912	0.005516425	0.95200708	0.005516425				
2.004897269	0.005837028	0.964205031	0.005837028				
1.580294059	0.006152977	0.972990688	0.006152977				
1.25897559	0.00646557	0.97938814	0.00646557				

7	8	5	8				
1.012939735	0.006775737	0.984099228	0.006775737				
0.822458305	0.007084095	0.987607297	0.007084095				
0.673459946	0.007391108	0.990247894	0.007391108				
0.55578563	0.007697106	0.992256168	0.007697106				
0.46201453	0.008002328	0.993798597	0.008002328				
0.386665047	0.008306953	0.994994286	0.008306953				
0.325644881	0.008611113	0.995929332	0.008611113				
0.275868141	0.008914909	0.996666605	0.008914909				
0.234985727	0.009218416	0.997252469	0.009218416				
0.201193409	0.009521694	0.997721437	0.009521694				
0.173093751	0.009824787	0.998099428	0.009824787				
0.149595788	0.010127731	0.998406079	0.010127731				

0.129841428	0.010430553	0.998656387	0.010430553				
0.113150963	0.010733276	0.998861892	0.010733276				
0.098982385	0.011035917	0.999031542	0.011035917				
0.086900753	0.011338491	0.999172323	0.011338491				
0.076554952	0.011641008	0.999289725	0.011641008				
0.067659924	0.011943478	0.999388091	0.011943478				
0.059982995	0.012245909	0.999470873	0.012245909				

APPENDIX C: MATLAB SCRIPTS

Circular Midpoint Generator

```
clear;
clc;
close all;

%% Introduction
%This program is meant to facilitate development of the
amplitude, surface,
%and load of mesh cells in ABAQUS. This program creates an
excel file that
%has the midpoints for every cell in a circular column
subjected to load

%This program is meant to facilitate development of loading
conditions for
%circular columns in FEFLO based on an existing model in
ABAQUS. This
%program takes the inputs of the columns mesh size, first
row element
%numbers, associated surface numbers of those elements,
basic column
%geometry, and numerical incrementation element numbers per
row and outputs
%an excel file that contains the external midpoints for
every element in
%the column subjected to load.

%% Inputting Data
%The data should have 2 separate columns: The first should
detail element #,
%the 2nd the surface # ABAQUS assigns the element
data =
table2array(readtable('Sample_Circular_Column_Elements.xlsx
','ReadVariableNames',false));
datasize = size(data);
```

```
elenum = data(:,1);     %Inputting Element Numbers
surfnum = data(:,2);    %Inputting Surface numbers
associated with Element
Radius = 190.5;     %mm
Mesh = 50;      %mm
Column_Height = 7000;       %mm
ele_increment = 43;     %How much does the element number
increase as it goes up the column

%% Processing the Data
%This section develops 2 sets of charts; one for the first
layer on the
%column and one for every external element on the column.
The first layer
%is primarily based on the inputted data for element
numbers and surface
%numbers while the full chart is based on the first layer,
mesh, column
%height, and element increment. This program assumes that
the first element
%named is placed at x=0.

first_ele_count = datasize(1,1);        %How many external
elements are in the first layer
angle = 360/first_ele_count;            %Angle between
elements' midpoints
first_layer = zeros(first_ele_count,5); %first_layer is the
full data of the column's first layer
for i = 1:first_ele_count
    first_layer(i,1) = elenum(i,1);
%Element Number
    first_layer(i,2) = Radius*cosd(90+angle*(i-1));     %X-
Coordinate of Midpoint
    first_layer(i,3) = Radius*sind(90+angle*(i-1));     %Y-
Coordinate of Midpoint
    first_layer(i,4) = Mesh/2;                          %Z-
Coordinate of Midpoint
    first_layer(i,5) = surfnum(i,1);
%Element's Surface Number
end

ele_count = Column_Height*datasize(1,1)/Mesh;
full_chart = zeros(ele_count,5);
%full_chart documents every element's full data
iteration = 0;
```

```
count = 1;
%Because the data for the x&y coordinates and the surface
numbers is the
%same for the elements as they move up the z-axis, the only
data that
%changes is the z-coordinate and the element number. Thus,
the program
%executes an if-statement to ensure that when the chart
moves to a new layer,
%the data for the x/y coords and surface number stays the
same while the
%element number and z-coord changes.
for j = 1:ele_count
    full_chart(j,1) = elenum((j-
iteration*first_ele_count),1)+ele_increment*iteration;
    full_chart(j,2) = Radius*cosd(90+angle*(j-1));
    full_chart(j,3) = Radius*sind(90+angle*(j-1));
    full_chart(j,4) = Mesh/2+Mesh*iteration;
    full_chart(j,5) = surfnum((j-
iteration*first_ele_count),1);
    count = count+1;
    if count == first_ele_count+1
        iteration=iteration+1;
        count = 1;
    end
end

%% Reorganizing the Data
%The data should be separated via surface numbers to make
development of
%surface loads easier when they come back
%Every element in ABAQUS has 6 surface numbers, thus 6
charts should be
%made. For the purposes of this program, 2 charts will
inevitable be empty
%due to 2 of the surface numbers being applied to the axial
faces of the
%column which haven't been accounted for in this program.
The final_chart
%combines all of the charts together organized by surface
number, then by
%z-coordinate
Chart1 = zeros(sum(full_chart(:,5) == 1),4);
Chart2 = zeros(sum(full_chart(:,5) == 2),4);
Chart3 = zeros(sum(full_chart(:,5) == 3),4);
```

```
Chart4 = zeros(sum(full_chart(:,5) == 4),4);
Chart5 = zeros(sum(full_chart(:,5) == 5),4);
Chart6 = zeros(sum(full_chart(:,5) == 6),4);

%Used to iterate through surface-dictated charts
i1 = 1;
i2 = 1;
i3 = 1;
i4 = 1;
i5 = 1;
i6 = 1;

%For-Loop to iterate through full chart and populate
surface-dictated
%charts whenever an element with the corresponding surface
number is found
for k = 1:ele_count
    if full_chart(k,5) == 1
        Chart1(i1,1) = full_chart(k,1);
        Chart1(i1,2) = full_chart(k,2);
        Chart1(i1,3) = full_chart(k,3);
        Chart1(i1,4) = full_chart(k,4);
        i1 = i1+1;
    elseif full_chart(k,5) == 2
        Chart2(i2,1) = full_chart(k,1);
        Chart2(i2,2) = full_chart(k,2);
        Chart2(i2,3) = full_chart(k,3);
        Chart2(i2,4) = full_chart(k,4);
        i2 = i2+1;
    elseif full_chart(k,5) == 3
        Chart3(i3,1) = full_chart(k,1);
        Chart3(i3,2) = full_chart(k,2);
        Chart3(i3,3) = full_chart(k,3);
        Chart3(i3,4) = full_chart(k,4);
        i3 = i3+1;
    elseif full_chart(k,5) == 4
        Chart4(i4,1) = full_chart(k,1);
        Chart4(i4,2) = full_chart(k,2);
        Chart4(i4,3) = full_chart(k,3);
        Chart4(i4,4) = full_chart(k,4);
        i4 = i4+1;
    elseif full_chart(k,5) == 5
        Chart5(i5,1) = full_chart(k,1);
        Chart5(i5,2) = full_chart(k,2);
        Chart5(i5,3) = full_chart(k,3);
```

```
        Chart5(i5,4) = full_chart(k,4);
        i5 = i5+1;
    elseif full_chart(k,5) == 6
        Chart6(i6,1) = full_chart(k,1);
        Chart6(i6,2) = full_chart(k,2);
        Chart6(i6,3) = full_chart(k,3);
        Chart6(i6,4) = full_chart(k,4);
        i6 = i6+1;
    end
end

%% Putting it Together
%The result of this part of the program is to develop the
full midpoints
%chart separated by surface number
final_chart = [Chart1;Chart2;Chart3;Chart4;Chart5;Chart6];
```

Full ABAQUS Definition Creator For Side S1

```
clear;
clc;
close all;

%% Introduction
%This program is meant to facilitate development of the
amplitude, surface,
%and load of mesh cells in ABAQUS

%% Importing Data & Preparing Text Output
data = table2array(readtable('Sample Amplitudes.xlsx'));
datasize = size(data);
fileID = fopen('C:\Users\Jacob Sanders\Documents\ABAQUS
Matlab Script\ABAQUS_Input_Setup.txt', 'w');
%This assumes that the first row refers to the elements and
the first
%column refers to the time steps. If this changes, the
table needs to be
%changed to reflect that

%% Surface Generation

for elenum = 2:datasize(1,2)
```

```
    %Many of the routines in this script refer to
'data(1,elenum)'. This
    %term takes the first row of the table (the element
numbers) and runs
    %them through a for-loop that create a display
statement to follow the
    %template below.

    formatSpec = '*Elset, elset="_Element %d X Side_S1",
internal, instance=Part-1-1\r\n';
    fprintf(fileID,formatSpec,data(1,elenum));
    fprintf(fileID,'%d,\r\n',data(1,elenum));
end
%*Elset, elset="_Element 1 X Side_S2", internal,
instance=PART-1-1
%  1,

for elenum = 2:datasize(1,2)
    %Many of the routines in this script refer to
'data(1,elenum)'. This
    %term takes the first row of the table (the element
numbers) and runs
    %them through a for-loop that create a display
statement to follow the
    %template below.

    formatSpec = '*Elset, elset="_Element %d X Side_S1",
internal, instance=Part-1-1\r\n';
    fprintf(fileID,formatSpec,data(1,elenum));
    fprintf(fileID,'%d,\r\n',data(1,elenum));
    formatSpec = '*Surface, type=ELEMENT, name="Element %d
X Side" \r\n';
    fprintf(fileID,formatSpec,data(1,elenum));
    fprintf(fileID,'"_Element %d X Side_S1", S1
\r\n',data(1,elenum));
end
fprintf(fileID,'\r\n');
%Trying to emulate the following template with different
elements
%*Elset, elset="_Element 1 X Side_S2", internal,
instance=PART-1-1
%  1,
% *Surface, type=ELEMENT, name="Element 1 X Side"
% "_Element 1 X Side_S2", S2
```

```
%% Amplitude

for elenum = 2:datasize(1,2)
    formatSpec = '*Amplitude, name=Amplitudex%d, time=TOTAL
TIME\r\n';
    fprintf(fileID,formatSpec,data(1,elenum));
    for timestep = 2:datasize(1,1)-1
        formatSpec = '%10.8f, %9.2f,';

fprintf(fileID,formatSpec,data(timestep,1),data(timestep,el
enum));
        fprintf(fileID,'\r\n');
    end
    %data(timestep,1) gets the time value of the chosen
element at the
    %timestep specified while data(timestep,elenum) gets
the amplitude at
    %that timestep. Thus the template shown is thus:
    %'time'.,       'amplitude'.,
    %This template only changes at the end of the amplitude
chain, in which
    %case the final amplitude value drops the comma.
    formatSpec = '%10.8f, %9.2f';

fprintf(fileID,formatSpec,data(timestep+1,1),data(timestep+
1,elenum));
    fprintf(fileID,'\r\n');
end
%Trying to emulate the following template with different
amplitudes
%     *Amplitude, name=RANDOMAMP, time=TOTAL TIME
%     0.,               1.,
%     2.,              10.,
%     4.,               4.,
%     6.,              20.,
%     8.,               5.,
%     10.,              0.



%% Loads
fprintf(fileID,'\r\n');
fprintf(fileID,'**\r\n');
fprintf(fileID,'** LOADS\r\n');
fprintf(fileID,'**\r\n');
```

```
for elenum = 2:datasize(1,2)

    formatSpec = '** Name: SURFFORCEx-%d   Type:
Pressure\r\n';
    fprintf(fileID,formatSpec,data(1,elenum));

    formatSpec = '*Dsload, amplitude=Amplitudex%d\r\n';
    fprintf(fileID,formatSpec,data(1,elenum));

    formatSpec = '"Element %d X Side", P, 1e-07\r\n';
    fprintf(fileID,formatSpec,data(1,elenum));
end
%Due to the Load definition relying on the amplitude and
surface titles, a
%hiccup could occur where the definitions aren't referred
to correctly
%(usually due to a mistyping of the load definition)
%This could be avoided by storing all of the surface and
amplitude titles
%in a bank, however that is a bit superfluous and would
cause the program
%to take longer. Diligence in coding is advised.
% ** Name: SURFFORCE-2   Type: Pressure
% *Dsload, amplitude=TRIANGULAR
% "Element 1 X Side", P, 2e+06
```

REFERENCES

1. Cole, R.H.; Weller, R. Underwater Explosions. Phys. Today **1948**, 1, 35. [Google Scholar] [CrossRef]
2. Costanzo, F.A. Underwater Explosion Phenomena and Shock Physics. In Structural Dynamics; Proulx, T., Ed.; Springer: New York, NY, USA, 2011; Volume 3, pp. 917–938. [Google Scholar]
3. Cooper, P.W. Explosives Engineering; John Wiley & Sons: Hoboken, NJ, USA, 2018. [Google Scholar]
4. Evans, A. Structural Response in Underwater Explosions; George Mason University: Fairfax, VA, USA, 2017. [Google Scholar]
5. Hsu, C.-Y.; Liang, C.-C.; Nguyen, A.-T.; Teng, T.-L. A numerical study on the underwater explosion bubble pulsation and the collapse process. Ocean. Eng. **2014**, 81, 29–38. [Google Scholar] [CrossRef]
6. Ming, F.; Zhang, A.; Xue, Y.; Wang, S. Damage characteristics of ship structures subjected to shockwaves of underwater contact explosions. Ocean. Eng. **2016**, 117, 359–382. [Google Scholar] [CrossRef]
7. Brett, J.M.; Buckland, M.; Turner, T.; Killoh, C.G.; Kiernan, P. An Experimental Facility for Imaging of Medium Scale Underwater Explosions. Defence Science and Technology Organisation Victoria (Australia) Platform Sciences Lab. 1 May 2003. Available online: https://apps.dtic.mil/sti/citations/ADA417894 (accessed on 1 August 2021).

8. Loomis, J.B. Impact of Underwater Explosions on Concrete Bridge Foundations. Naval Postgraduate School Monterey ca Monterey United States. 1 June 2016. Available online: https://apps.dtic.mil/sti/citations/AD1026694 (accessed on 1 August 2021).
9. Vanadit-Ellis, W.; Davis, L.K. Physical modeling of concrete gravity dam vulnerability to explosions. In Proceedings of the 2010 International WaterSide Security Conference, Carrara, Italy, 3–5 November 2010; pp. 1–11. [Google Scholar]
10. De, A.; Niemiec, A.; Zimmie, T.F. Physical and Numerical Modeling to Study Effects of an Underwater Explosion on a Buried Tunnel. J. Geotech. Geoenviron. Eng. **2017**, 143, 04017002. [Google Scholar] [CrossRef]
11. Huang, C.; Liu, M.; Wang, B.; Zhang, Y. Underwater explosion of slender explosives: Directional effects of shock waves and structure responses. Int. J. Impact Eng. **2019**, 130, 266–280. [Google Scholar] [CrossRef]
12. Urgessa, G.; Lohner, R. Preliminary Efforts in Validation of Feflo for Underwater Explosion; Auburn University: Aubur, AL, USA, 2020. [Google Scholar]
13. Wang, P.; Zhang, Z.; Yan, Q.; Zhang, C. A substructure method for the transient response of vertical cylinders subjected to shock wave of underwater explosion. Ocean. Eng. **2020**, 218, 108128. [Google Scholar] [CrossRef]
14. Mair, H.U. Review: Hydrocodes for Structural Response to Underwater Explosions. Shock. Vib. **1999**, 6, 81–96. [Google Scholar] [CrossRef]

15. Collins, G.S. An Introduction to Hydrocode Modeling; Imperial College London: London, UK, 2002; pp. 2–11. [Google Scholar]

16. Liu, M.; Liu, G.R.; Lam, K.Y.; Zong, Z. Smoothed particle hydrodynamics for numerical simulation of underwater explosion. Comput. Mech. **2003**, 30, 106–118. [Google Scholar] [CrossRef]

17. Afrasiabi, M.; Mohammadi, S. Analysis of bubble pulsations of underwater explosions by the smoothed particle hydro-dynamics method. In Proceedings of the ECCOMAS International Conference on Particle Based Methods, Barcelona, Spain, 25–27 November 2009. [Google Scholar]

18. Zhang, Z.; Wang, L.; Silberschmidt, V.V. Damage response of steel plate to underwater explosion: Effect of shaped charge liner. Int. J. Impact Eng. **2017**, 103, 38–49. [Google Scholar] [CrossRef]

19. Gannon, L. Simulation of underwater explosions in close-proximity to a submerged cylinder and a free-surface or rigid boundary. J. Fluids Struct. **2019**, 87, 189–205. [Google Scholar] [CrossRef]

20. Ren, X.; Shao, Y. Numerical Investigation on Damage of Concrete Gravity Dam during Noncontact Underwater Explosion. J. Perform. Constr. Facil. **2019**, 33, 04019066. [Google Scholar] [CrossRef]

21. Moradloo, A.J.; Adib, A.; Pirooznia, A. Damage analysis of arch concrete dams subjected to underwater explosion. Appl. Math. Model. **2019**, 75, 709–734. [Google Scholar] [CrossRef]

22. Hai, L.; Ren, X. Computational investigation on damage of reinforced concrete slab subjected to underwater explosion. Ocean. Eng. **2020**, 195, 106671. [Google Scholar] [CrossRef]

23. Zhao, X.; Wang, G.; Lu, W.; Yan, P.; Chen, M.; Zhou, C. Damage features of RC slabs subjected to air and underwater contact explosions. Ocean. Eng. **2018**, 147, 531–545. [Google Scholar] [CrossRef]

24. Yang, G.; Wang, G.; Lu, W.; Zhao, X.; Yan, P.; Chen, M. Cross-section shape effects on anti-knock performance of RC columns subjected to air and underwater explosions. Ocean. Eng. **2019**, 181, 252–266. [Google Scholar] [CrossRef]

25. Zhuang, T.-S.; Wang, M.-Y.; Wu, J.; Yang, C.-Y.; Zhang, T.; Gao, C. Experimental investigation on dynamic response and damage models of circular RC columns subjected to underwater explosions. Def. Technol. **2020**, 16, 856–875. [Google Scholar] [CrossRef]

26. Yan, Q.; Liu, C.; Wu, J.; Zhuang, T. Experimental and Numerical Investigation of Reinforced Concrete Pile Subjected to Near-Field Non-Contact Underwater Explosion. Int. J. Struct. Stab. Dyn. **2020**, 20, 2040003. [Google Scholar] [CrossRef]

27. Liaw, C.-Y.; Chopra, A.K. Dynamics of towers surrounded by water. Earthq. Eng. Struct. Dyn. **1974**, 3, 33–49. [Google Scholar] [CrossRef]

28. *Home*. Omaha District > About > Centers of Expertise > Protective Design Center > PDC Software. (n.d.). Retrieved May 4, 2022, from

https://www.nwo.usace.army.mil/About/Centers-of-Expertise/Protective-Design-Center/PDC-Software/

29. Material damping - Massachusetts institute of technology. (n.d.). Retrieved May 4, 2022, from https://abaqus-docs.mit.edu/2017/English/SIMACAEMATRefMap/simamat-c-dampingopt.htm
30. Rainald Lohner, Advances in FEFLO, 51st AIAA Aerospace Sciences Meeting including the New Horizons Forum and Aerospace Exposition, 373, 2013
31. Urgessa, G., Horton, S., Taha, M. R., & Maji, A. (2005). Significance of Stress-block Parameters on the Moment Capacity of Sections Under-reinforced with FRP. *Special Publication*, *230*, 1531-1550.
32. Choi, K. K., Urgessa, G., Taha, M. M., & Maji, A. K. (2008). Quasi-balanced failure approach for evaluating moment capacity of FRP underreinforced concrete beams. *Journal of Composites for Construction*, *12*(3), 236-245.
33. Collins, M. P., Mitchell, D., & MacGregor, J. G. (1993). Structural design considerations for high-strength concrete. *Concrete international*, *15*(5), 27-34.
34. Popovics, S. (1973). A numerical approach to the complete stress-strain curve of concrete. *Cement and concrete research*, *3*(5), 583-599.
35. Belarbi, A., & Hsu, T. T. (1994). Constitutive laws of concrete in tension and reinforcing bars stiffened by concrete. *Structural Journal*, *91*(4), 465-474.
36. Lubliner, J., Oliver, J., Oller, S., & Oñate, E. (1989). A plastic-damage model for concrete. *International Journal of solids and structures*, *25*(3), 299-326.

37. Lee, J., & Fenves, G. L. (1998). Plastic-damage model for cyclic loading of concrete structures. *Journal of engineering mechanics*, *124*(8), 892-900.

38. Karsan, I. D., & Jirsa, J. O. (1969). Behavior of concrete under compressive loadings. *Journal of the Structural Division*, *95*(12), 2543-2564.

39. Gopalaratnam, V. S., & Shah, S. P. (1985, May). Softening response of plain concrete in direct tension. In *Journal Proceedings* (Vol. 82, No. 3, pp. 310-323).

40. Swisdak Jr, M. M. (1978). *Explosion effects and properties. Part II. Explosion effects in water*. Naval Surface Weapons Center White Oak Lab Silver Spring MD.

41. Keevin, T. M., & Hempen, G. L. (1997). *The environmental effects of underwater explosions with methods to mitigate impacts*. CORPS OF ENGINEERING ST LOUIS MO ST LOUIS DISTRICT.

42. Michał, S., & Andrzej, W. (2015, August). Calibration of the CDP model parameters in Abaqus. In *The 2015 Wourld Congress on Advances in Structural Engineering and Mechanics (ASEM15)*.

43. Kwon, Y. W., & Fox, P. K. (1993). Underwater shock response of a cylinder subjected to a side-on explosion. *Computers & structures*, *48*(4), 637-646.

BIOGRAPHY

Jacob Sanders graduated from South County High School, Lorton, Virginia, in 2016. He received his Bachelor of Science in Mechanical Engineering from George Mason University in 2020. He was employed as a Graduate Research Assistant for George Mason University and received his Masters of Science in Civil and Infrastructure Engineering at George Mason University in 2022.